

# **Advanced Electromagnetic Wave Technologies for the Detection of Abandoned Mine Entries and Delineation of Barrier Pillars**

**by**

**Larry G. Stolarczyk, Sc.D., President  
Stolar Horizon, Inc., Raton, New Mexico**

**Syd S. Peng, Ph.D., C.T. Holland Professor, Chairman  
Department of Mining Engineering,  
West Virginia University, Morgantown, West Virginia**

**Presented to**

**Mine Safety and Health Administration (MSHA) and  
Office of Surface Mining Reclamation and Enforcement (OSMRE)**

**Interactive Forum on Geophysical Technologies for  
Detecting Underground Coal Mine Voids**

**July 28–30, 2003**

**Lexington, Kentucky**

# Contents

Abstract.....	1
Introduction.....	2
Radar Instrumentation.....	15
Electromagnetic Fields in the Coal Seam.....	20
Coal Seam Vision with the Radio Imaging Method (RIM).....	22
Void Detection with Electromagnetic Wave Methods.....	26
Stolar Radio Imaging Method in Void Detection.....	26
3-D RIM to Locate and Image Mine Voids.....	26
Principles of Void Detection with RIM.....	26
3-D RIM Configurations.....	28
In-Mine 3-D RIM Survey Instrumentation.....	28
Downhole Survey Equipment.....	29
Phase Synchronization.....	32
RIM Method 1: Fence-Line Confirmation of Barrier Pillar.....	33
Fence-Line Survey Plan.....	34
RIM Method 2: Tomographic Imaging of Mine Workings.....	35
RIM Tomography Survey Plan.....	36
RIM Tomography Survey Results.....	38
RIM Case Study.....	39
Case Study Survey Procedure.....	40
Case Study Survey Results.....	41
Void Detection and Confirmation Electromagnetic Wave Instrumentation Under Development.....	43
Proposed In-Mine Test Site.....	49
Drillstring Radar (DSR) for In-Seam Guidance and Navigation.....	50
Current In-Seam Drilling Technology.....	52
Basic Structure of the Drillstring Radar (DSR) Tool.....	54
Major Subsystems.....	56
Concluding Remarks.....	57
References.....	58
Acknowledgments.....	61

# Figures

1.	Traveling EM waves are composed of electric (E) and orthogonal magnetic (H) fields .....	2
2.	Phase shift concept of travel distance .....	4
3.	Energy flow in the void detection problem.....	5
4.	Transmitting antenna sources .....	7
5.	Traveling electric field components illustrate the tilt in the vertical electric field component .....	8
6.	Secondary magnetic fields from a void .....	9
7.	Surface EM gradiometer response over a void .....	10
8.	Survey line across a dam.....	11
9.	Attenuation rate (dB/ft) versus frequency.....	12
10.	Electrical conductivity in Siemens per meter versus frequency .....	13
11.	Anisotropic gas flow permeability and dielectric ( $\epsilon$ ) constant of coal .....	14
12.	Short-duration pulse radar waveform .....	15
13.	Radar instrumentation.....	17
14.	Radar with a directional coupler .....	18
15.	Natural waveguide for EM wave transmission.....	20
16.	Coal seam EM wave attenuation rate versus frequency .....	21
17.	Coal seam EM wave attenuation rate versus boundary rock conductivity ....	21
18.	Sensitivity of radio waves to changes in coal layer thickness .....	22
19.	Natural coal seam anomalies .....	23
20.	Cross section of a paleochannel.....	23
21.	Comparison of RIM image reconstruction methods.....	24
22.	Image of a paleochannel in a 1,000-ft-wide longwall panel.....	25
23.	Normal attenuation rates for water-filled, air-filled, and coal waveguides ...	27
24.	In-mine instrumentation.....	28
25.	In-Mine RIM-IV transmitter.....	29
26.	Crosswell RIM-IV reduces drilling cost.....	29
27.	Crosswell detection of a coal seam void.....	30
28.	The RIM downhole probes are lowered into vertical borings using fiber-optic cable. Stolar's RIM Instrumentation Trailer contains two (2) cable hoists, control electronics, and probe inventory. ....	31

## Figures (concluded)

29.	Receiver probe for the Downhole RIM-IV system deployed for field-testing.....	32
30.	Map of a mine’s target area .....	33
31.	Diagram of RIM survey site .....	34
32.	Map of the old workings originating from a highwall bench .....	36
33.	Map of a recommended survey plan at an old-workings site .....	37
34.	Location and borehole pattern of tomography grid over a suspected dike....	38
35.	Two-dimensional images for a 2000-ft tomography survey grid over a dike at a 1000-ft hole-to-hole separation .....	39
36.	Diagram of the survey area showing downhole boring location, in-mine receiver station, and transmission ray path.....	41
37.	Diagram of survey area showing contour map of RIM signal attenuation rate.....	42
38.	Detecting coal-rock interface horizons .....	43
39.	Cutting drum look-ahead radar sensor.....	44
40.	MSHA flameproof approved RMPA Horizon Sensor (HS-3) mounted on a coal cutting drum.....	45
41.	Horizon Sensor response.....	45
42.	Quecreek Mine breach .....	46
43.	Salt block simulation of a coal barrier pillar.....	47
44.	Results from the experiments in salt.....	48
45.	Dielectric constant measured with the Resonant Microstrip Patch Antenna (RMPA).....	49
46.	In-mine demonstration site .....	50
47.	Radar mapping of voids and geologic anomalies from vertical boreholes....	51
48.	Detection and imaging of abandoned coal mines along boreholes.....	51
49.	Vertical cross section of a coal bed illustrating conventional “sidetrack” trial-and-error drilling under a paleochannel as well as the down-the-hole drill motor .....	53
50.	Stolar Drillstring Radar (DSR) .....	54
51.	Measurements-While-Drilling (MWD) drillstring radar .....	54
52.	Block diagram of the drillstring radar instrumentation system .....	55

# **Advanced Electromagnetic Wave Technologies for the Detection of Abandoned Mine Entries and Delineation of Barrier Pillars**

**By Larry G. Stolarczyk, Sc.D.  
Syd S. Peng, Ph.D.**

## **Abstract**

The current high level of coal production is rapidly depleting easily minable coal reserves. Future mining will gradually concentrate in thinner, deeper, and geologically adverse coal seams. Some of the mining projects will be near old works where geophysical mapping methods will be applied separately or in conjunction with drilling techniques to delineate barrier pillars and detect voids ahead of mining machines. Several electromagnetic (EM) wave methods of detection and imaging of voids, impoundment leakage pathways, and geologic anomalies in coal beds have been investigated in recent years. Surface-based survey methods include magnetotelluric and local transmitters using low frequencies and radar at high frequencies. Both reflection and transmission instrumentation have been developed for surface, borehole, and in-mine applications.

This paper has been written for decision-makers in the coal mining industry who are concerned with the detection, confirmation, and mitigation of mining hazards in advance of mining. First, a practical insight into the science of EM wave energy travel in the coal bed has been prepared to give an understanding of EM wave interaction with voids, leakage pathways, oil/gas well casings, and geologic anomalies. Second, the interaction forms observables that are detected with specialized instrumentation. The surface-based instrumentation includes EM gradiometers and radar; in-mine and borehole instrumentation includes radar and the Radio Imaging Method (RIM). This paper also describes the development of radar for horizontal directional drills and cutting drums.

# Introduction

The electromagnetic (EM) theory underlying all of the void and geologic anomaly detection methods is based upon the propagation of EM wave energy from a transmitting source of EM waves to a companion receiver (1–5). In the case of the magnetotelluric surface probing methods, the transmitting sources are naturally occurring, such as lightning, earth-ionosphere resonances, and sun spots (6). The traveling EM waves are composed of transverse electric and magnetic field components, as illustrated in Figure 1.

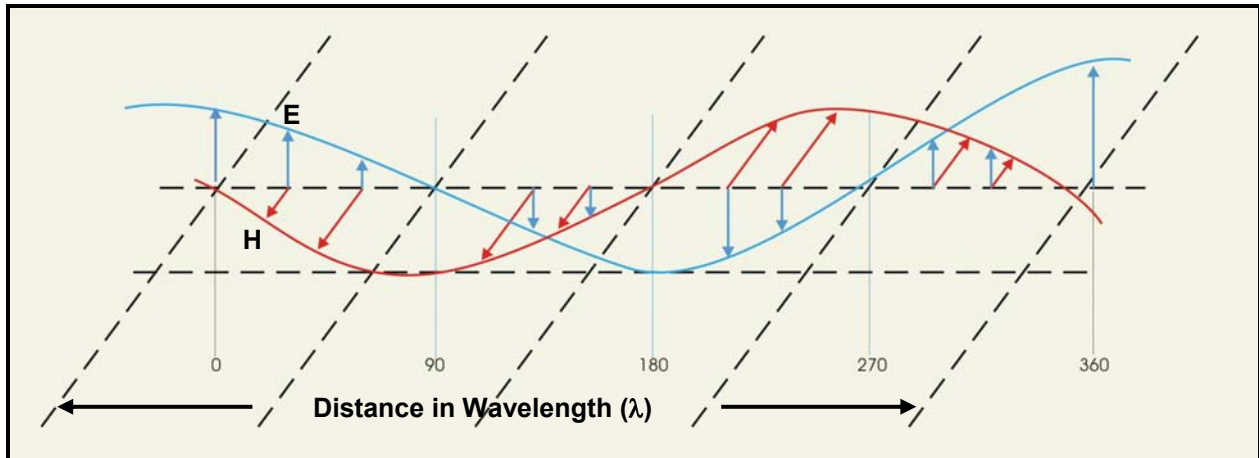


**Figure 1.** Traveling EM waves are composed of electric (E) and orthogonal magnetic (H) fields

The traveling field components continually exchange energy between the electric and magnetic fields along the transmission path. The distance traveled for the energy to be completely transferred to the other field component and back again is a wavelength ( $\lambda$ ), mathematically represented by

$$\lambda = \frac{C}{f\sqrt{\epsilon_r}} \text{ in meters} \quad (1)$$

where  $C = 3 \times 10^8$  is the speed of light in meters per second,

$f$  = the frequency of the energy exchange in Hertz,

and  $\epsilon_r$  = the relative dielectric constant of the natural media.

The electric and magnetic fields can be mathematically represented by sinusoidal waveforms that shift in phase by 360 electrical degrees when traveling a distance of one wavelength. The fields illustrated in Figure 1 are detected with receiving antennas. A short vertical electrical conductor is called an electric dipole and will reproduce an electromotive force (emf) voltage waveform similar to the electric field waveform mathematically expressed as

$$\text{emf} = h_{ef} E = M \cos \omega t \quad (2)$$

where  $h_{ef}$  = the effective height of the antenna,

$E$  = the amplitude of the electric field in volts per meter,

$M$  = the magnitude of the sine wave signal,

$\omega = 2\pi f$  and  $f$  is the frequency in Hertz,

and  $t$  = the continuing time.

A small coil of wire will reproduce an emf voltage waveform similar to the magnetic field expressed as

$$\text{emf} = -i\omega N\mu AH \sin(\omega t) = M \sin(\omega t) \quad (3)$$

where  $N$  = the number of turns in the coil,

$i = \sqrt{-1}$ ,

$A$  = area of coil in square meters,

$\mu = \mu_r \mu_0$  is the magnetic permeability and  $\mu_0 = 4\pi \times 10^{-7}$  Farads per meter,

and  $H$  = the amplitude of magnetic field in Amperes per meter.

If the receiving antennas were stationary, the output voltage would be continuous sine or cosine waveform.

If the electric field antenna were moved a distance ( $d$ ) from its original location to a new location, the reproduced waveform would be mathematically represented by

$$\text{emf} = M \cos [\omega t + \theta] \quad (4)$$

where  $\theta = d \left( \frac{2\pi}{\lambda} \right)$  is the phase shift (or rotation angle) in radians and one radian is 57 electrical degrees.

When the receiver moves one wavelength from its original position, the phase shift is  $2\pi$  or 360 electrical degrees.

Distance in the natural media can be determined by designing instrumentation to measure phase shift

$$\theta = d \left( \frac{2\pi}{\lambda} \right) \text{ in radians.} \quad (5)$$

The braced term is called the phase constant

$$\beta = \frac{2\pi}{\lambda} \text{ radians per meter} \quad (6)$$

and characterizes natural media.

Phase shift (or rotation angle) measurements are carried out with synchronized instrumentation. The concept of synchronization in mechanical and electronic systems is similar. For example, the cosine wave at the first location is called the reference signal. The reference signal is compared to the signal at the second location to determine the phase shift in radians.

An analogy of phase shift in EM fields traveling along a path through natural media is the rotation of a wagon wheel traveling along a path between the transmitter (source) to the receiver (Figure 2).

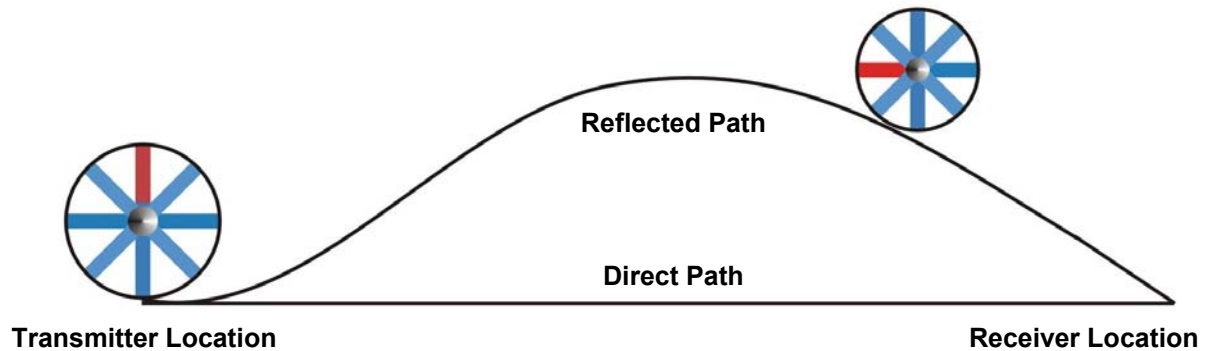


**Figure 2.** Phase shift concept of travel distance

As the wagon wheel rolls from the transmitter along a path (track) to the receiver, the red spoke angular rotation in degrees can be related to travel distance. In uniform natural media, the track is a straight line. The travel path of an EM wave is not always straight. EM fields are refracted when traveling near geologic anomalies where velocity changes spatial position. When the EM field receiver is synchronized with the transmitter, the total path phase shift can be

measured, which is important in the problem of detecting voids and geologic anomalies ahead of mining.

The velocity of the EM field is at the speed of light in free space, but slows down in natural media. The velocity ( $v$ ) in a dielectric like coal is given as

$$v = \frac{C}{\sqrt{\epsilon_r}} \text{ in meters per second.} \quad (7)$$

In distance measurements, the receiver must be synchronized with the transmitter to enable the measurement of total phase shift.

Figure 3 illustrates how energy flows in natural media, such as soil, coal, and other natural media. Energy is partly transmitted and reflected when the electrical parameters of the media abruptly change. Energy is absorbed as heat in coal.

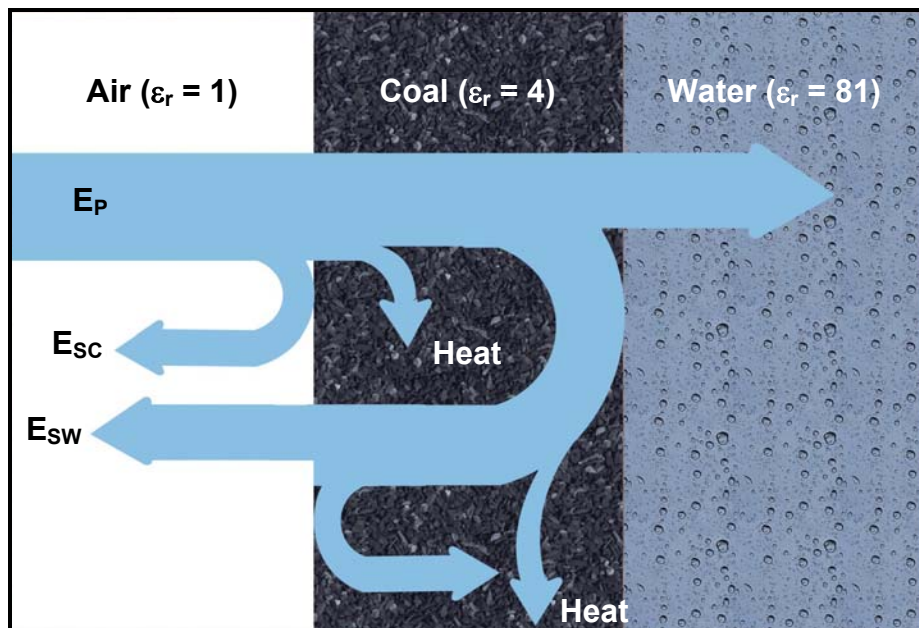


**Figure 3.** Energy flow in the void detection problem

Scattering of energy occurs when the void or anomaly is small compared with the wavelength. When the traveling primary EM wave (electric field  $E_p$ ) intersects a void or geologic anomaly, secondary EM waves (electric field  $E_s$ ) are formed. The secondary electric field traveling away from the air-coal interface is  $E_{sc}$ . The secondary field traveling from the coal-water interface is  $E_{sw}$ . Energy in the primary EM wave is converted to heat along the travel path and also transferred to the secondary EM fields. EM waves traveling nearby the anomaly are refracted. Because the secondary fields are only a small fraction of the magnitude of the primary fields, electronic instrumentation must be specifically developed to measure the secondary fields

in the presence of the much larger primary field. Everywhere in the natural medium, the total fields are represented by vectors as:

$$\text{Electric field} \quad \mathbf{E}_T = \mathbf{E}_p + \mathbf{E}_s \text{ and} \quad (8)$$

$$\text{Magnetic field} \quad \mathbf{H}_T = \mathbf{H}_p + \mathbf{H}_s. \quad (9)$$

The impedance ( $Z$ ) is the ratio of the total fields given as

$$\mathbf{Z} = \frac{\mathbf{E}_T}{\mathbf{H}_T}. \quad (10)$$

The transmitting antenna is the source of the primary EM fields. Low-frequency antennas are generally represented as point sources, as the physical size of these antennas is usually much smaller than their wavelength of operation and mathematically represented by dipoles (7, 8). Low frequencies are used in EM sources that operate on the earth's surface and transmit EM waves into the earth because longer wavelengths penetrate deeper in the ground. Long horizontal electric wires are electric dipoles, and loops (coils) of wire are magnetic dipoles. For frequencies in the 100s of MHz, microwave antennas are used as sources, but the depth of penetration of the signal from microwave antennas in the Earth is severely limited. The various types of transmitting sources are illustrated in Figure 4.

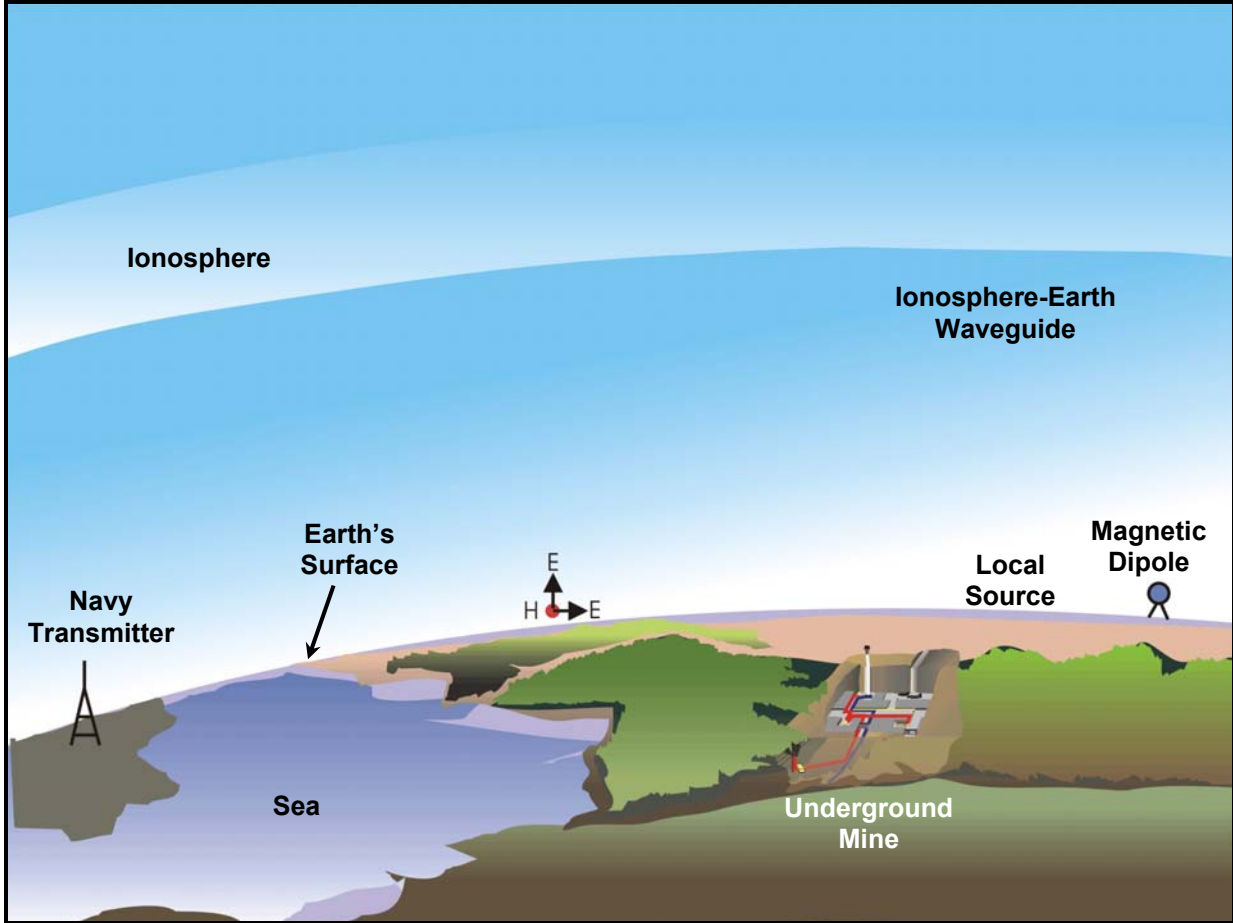


**Figure 4.** *Transmitting antenna sources*

Natural waveguides for transmission of EM waves include the earth-ionosphere waveguide illustrated in the above figure (9). The energy is transmitted with a vertically polarized electric (E) field and a horizontally polarized magnetic (H) field. The magnetic field is pointing into the page. At the air-earth interface, there is a small horizontally polarized electric field that lies on the earth's surface. The horizontally polarized E and H fields are responsible for the primary wave traveling vertically into the earth, as illustrated in Figure 5.

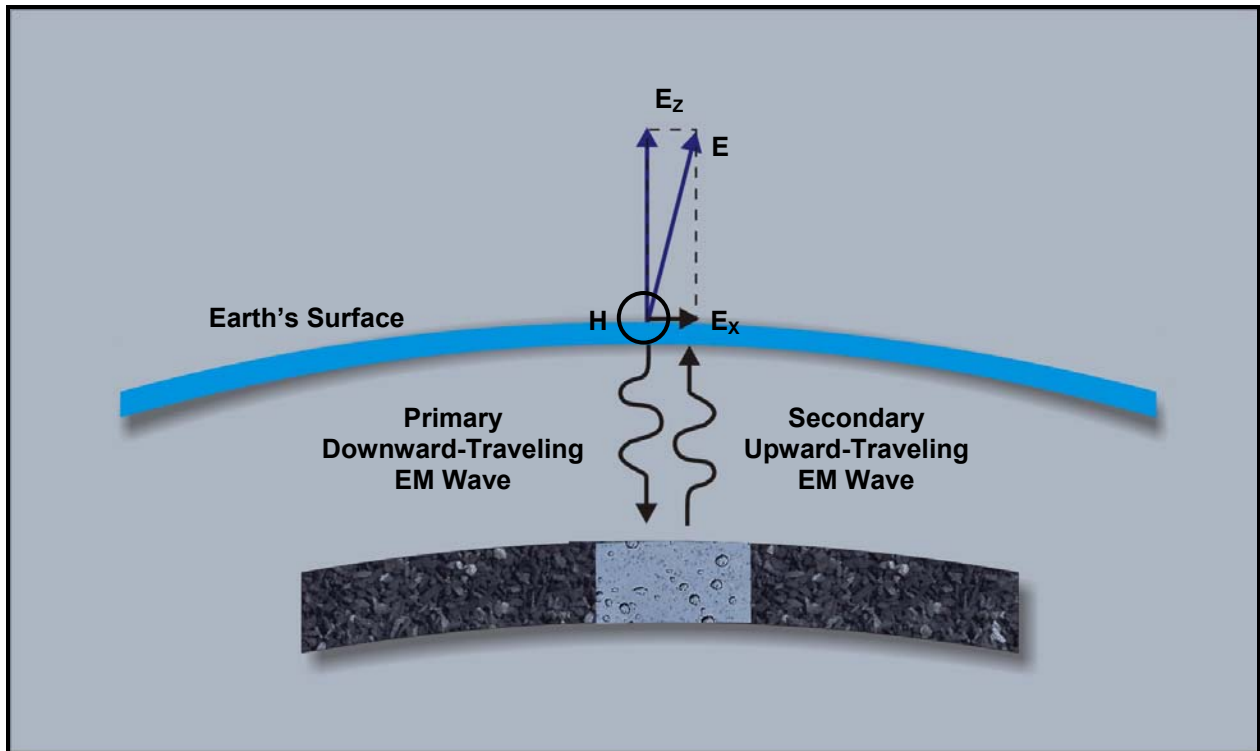


**Figure 5.** *Traveling electric field components illustrate the tilt in the vertical electric field component*

When the downward-traveling subsurface EM fields intersect a void or geologic anomaly, secondary fields form and travel back to the surface forming the total fields  $E_T$  and  $H_T$  at the surface. This causes the total horizontal electric field to change and the vertical electric field to tilt. The tilt would change over a void or geologic anomaly. The magnetotelluric instrumentation method measures the total horizontal electrical and magnetic field components. The surface impedance is recorded and graphically reconstructed along survey lines to form the observable in the magnetotelluric method.

EM gradiometer instrumentation has been developed for surface measurement (10). The DeltaEM gradiometer receiver is synchronized to the primary continuous wave magnetic fields traveling on the earth's surface. The DeltaEM receiver can be tuned to any frequency between 2 kHz and 2 MHz. Higher frequencies are used to detect smaller anomalies near the earth's surface. The primary wave is suppressed by more than 70 dB by differentially connected magnetic dipole antennas illustrated in Figure 6.

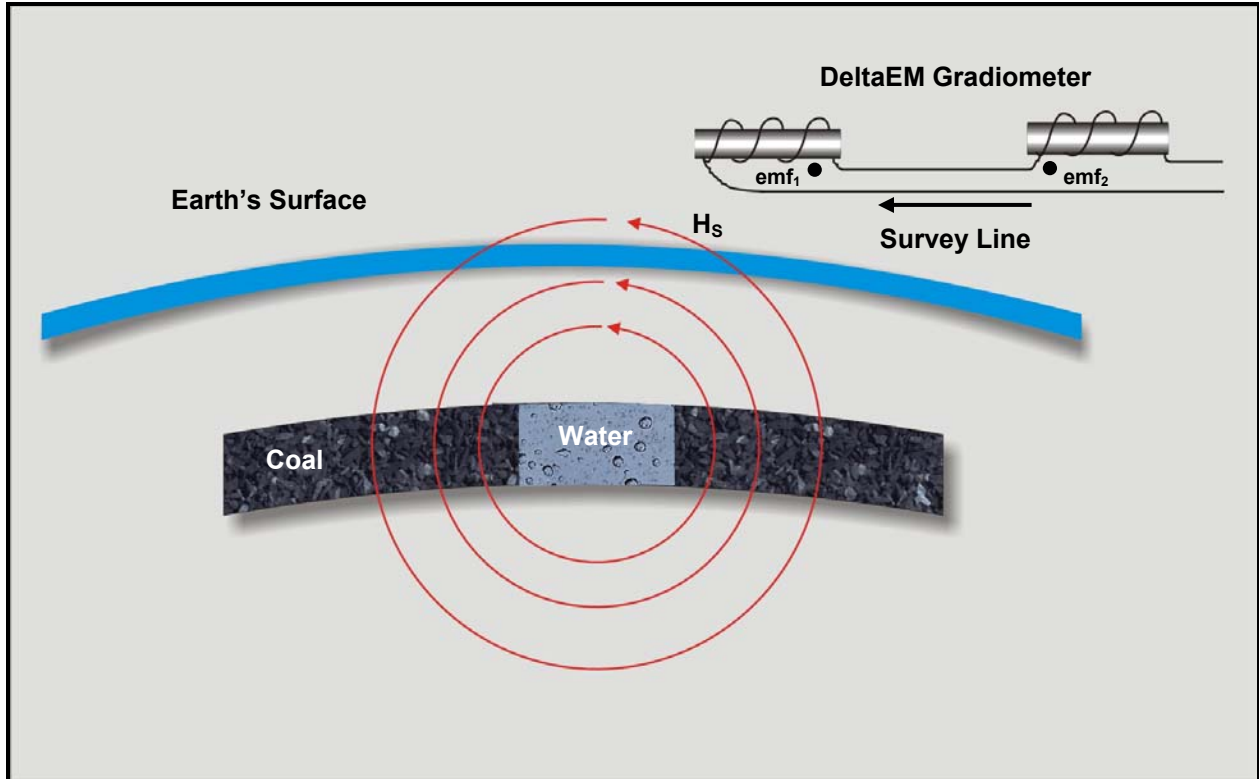


**Figure 6.** Secondary magnetic fields from a void

The differential ( $\nabla$ ) secondary wave is measured along the survey line crossing over the void. The scattered magnetic field component traveling away from the void is mathematically given by

$$H_s = \frac{\pi E_p}{i\omega \text{Ln}(\kappa\alpha)} \left( \frac{i\kappa}{2\pi r} \right)^{-1/2} e^{-i\kappa r} \quad (11)$$

where  $\kappa = \beta - i\alpha$ ,

$\alpha =$  the attenuation factor in Nepers per meter,

and  $H =$  a cylindrically spreading magnetic field in Amperes per meter.

Each magnetic dipole of the gradiometer array produces an output voltage given by  $emf_0 = emf_1 - emf_2$ .

The EM gradiometer response is illustrated in Figure 7.

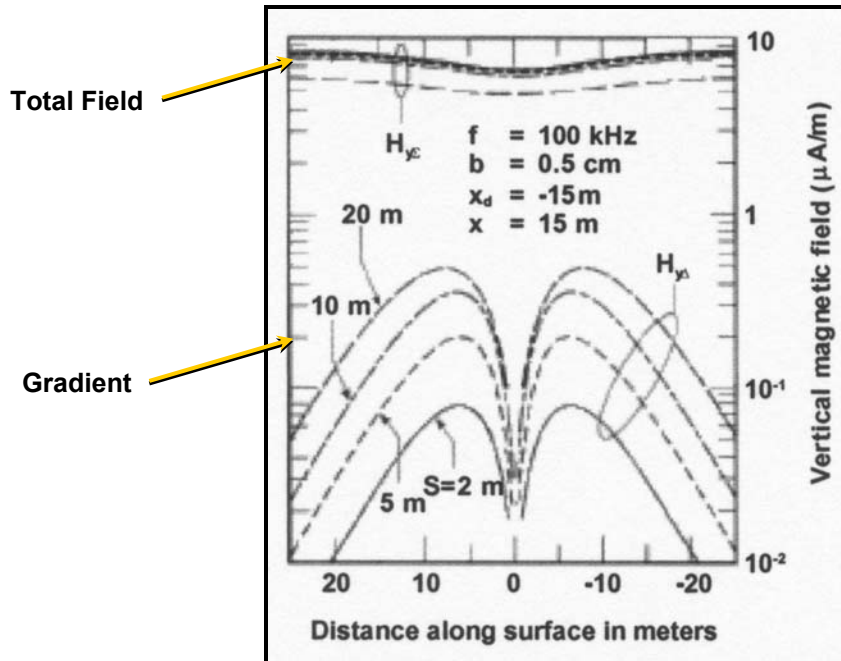


**Figure 7.** Surface EM gradiometer response over a void

The response illustrates the limitation in the surface-based EM measurement methods. Because the primary field is much larger than the secondary field, the total field changes by only a few percent when the survey line crosses over a significant geologic anomaly, whereas the gradient field changes by a significant amount. Surface-based instrumentation that measures total fields would exhibit poor resolution. The DeltaEM resolution is very high, which demonstrates that measuring resolution is not always related to wavelength. The wavelength in free space is 100,000 meters. The peak-to-peak separation is proportional to the depth of the anomaly (11). The DeltaEM instrumentation can be used over impoundment dams to detect leakage pathways and determine depth. A survey line across a dam is shown in Figure 8.

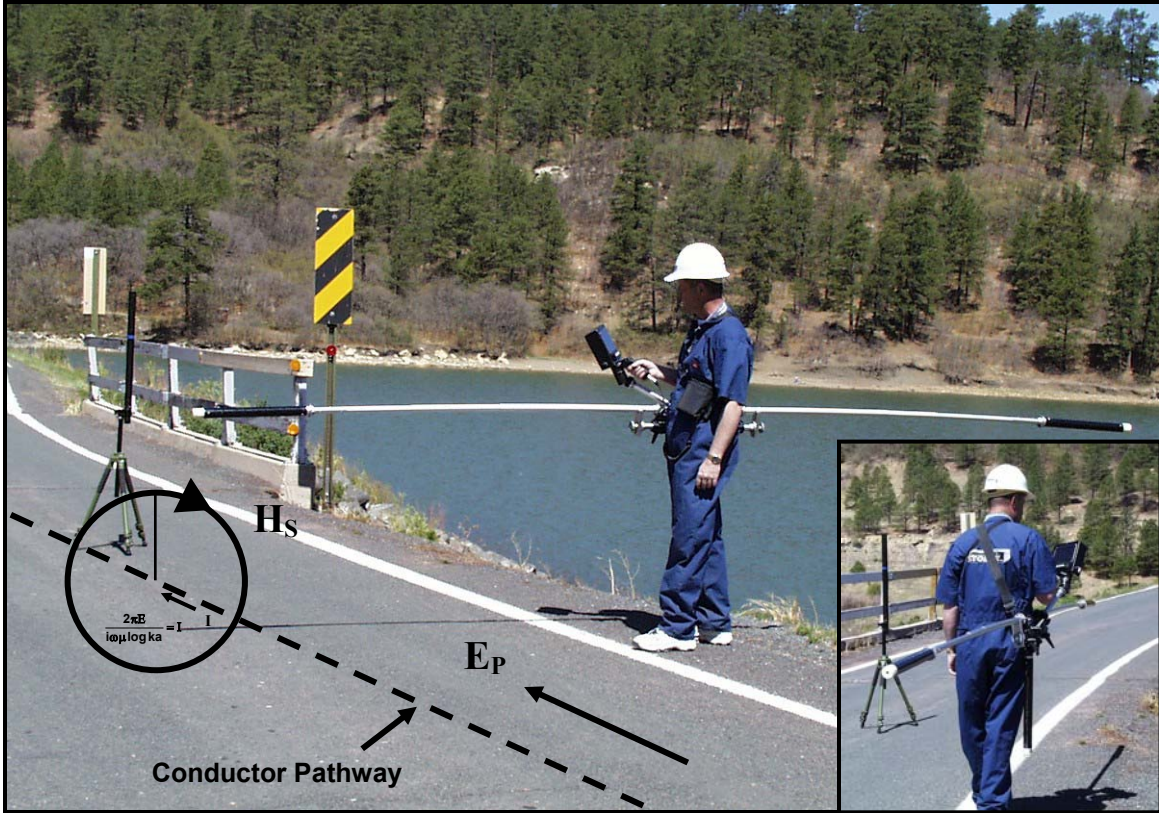


**Figure 8.** Survey line across a dam

Frequently asked questions are: “What is the depth of investigation?” and “What is the resolution?” The depth of investigation strongly depends on the attenuation rate given in units of Nepers per meter (ft) for the EM fields traveling in the media and the energy lost in creating the secondary electric and magnetic field vectors. A Neper is a unit of measure defining the decrease in magnitude over the travel distance. Oliver Heaviside (12) gives a formula for determining the attenuation rate as functions of frequency, and the electrical parameters of the natural media given as

$$\alpha = \omega \left[ \frac{\mu \epsilon}{2} \left( \sqrt{1 + \frac{\sigma^2}{\epsilon^2 \omega^2}} - 1 \right) \right]^{1/2} \text{ Nepers per meter} \quad (12)$$

$\sigma$  = the electrical conductivity in Siemens/meter (S/m),

$\epsilon$  =  $\epsilon_r \epsilon_0$  is the permittivity. The permittivity of free space  $\epsilon_0 = 1/36 \pi \times 10^{-9}$  Farads/meter, and  $\epsilon_r$  is the relative dielectric constant,

and  $\mu$  =  $\mu_r \mu_0$  is the magnetic permeability. The permeability of free space  $\mu_0 = 4 \pi \times 10^{-7}$ , and  $\mu_r$  is the relative permeability.

He also gave the phase shift (or rotation angle) as

$$\beta = \omega \left[ \frac{\mu\epsilon}{2} \left( \sqrt{1 + \frac{\sigma^2}{\epsilon^2\omega^2}} + 1 \right) \right]^{\frac{1}{2}} \text{ radians per meter.} \quad (13)$$

When the loss tangent given by  $\sigma/\omega\epsilon$  is much greater than unity  $\left(\frac{\sigma}{\omega\epsilon} \gg 1\right)$ , the attenuation rate is given by

$$\alpha = \beta = \sqrt{\frac{\omega\sigma\mu}{2}} \text{ Nepers per meter.} \quad (14)$$

When the loss tangent is much less than unity  $\left(\frac{\sigma}{\omega\epsilon} \ll 1\right)$ ,

$$\alpha = \frac{\sigma}{2} \sqrt{\frac{\mu}{\epsilon}} \text{ Nepers per meter,} \quad (15)$$

$$\beta = \omega\sqrt{\mu\epsilon}. \quad (16)$$

Figure 9 illustrates the attenuation rate as a function of frequency for a non-magnetic medium with a relative dielectric constant of 6.

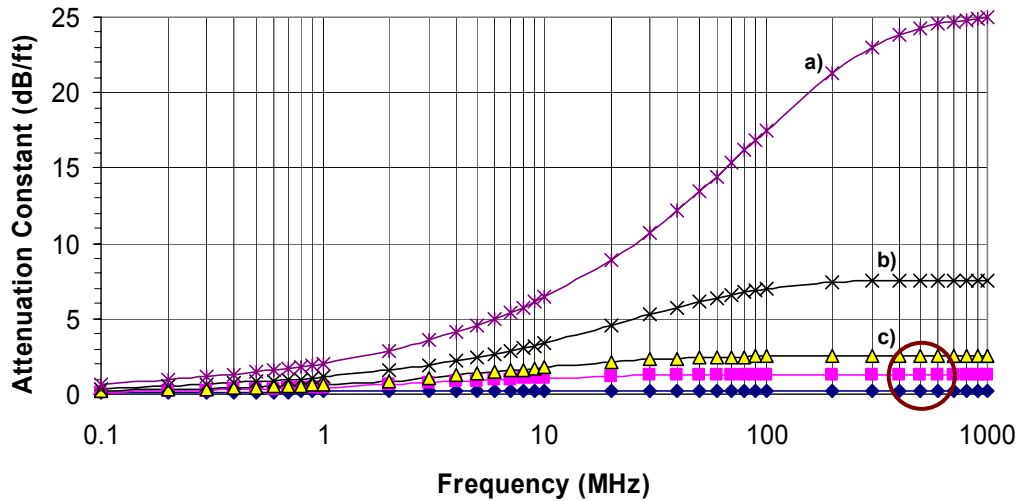


**Figure 9.** Attenuation rate (dB/ft) versus frequency exhibited by: a) shale/clay, b) coal with high moisture, c) range for US coals

The right side of the family of attenuation rate curves is where the loss tangent is greater than unity and the left side is where the loss tangent is much less than unity.

The significance of the loss tangent  $\sigma/\omega\epsilon$  is seen in Maxwell's first equation, given as

$$\nabla \times \mathbf{H} = \epsilon^* \frac{\partial \mathbf{E}}{\partial t} \quad (17)$$

where the rotating electric field component is represented by

$$\mathbf{E} = E_0 e^{+i\omega t} \quad (18)$$

and  $E_0$  is the magnitude of electric field.

The complex nature of the dielectric constant given by

$$\epsilon^* = \epsilon' - i\epsilon'' \quad (19)$$

where  $\epsilon'$  is the real part and  $\epsilon''$  is the imaginary part (13). Maxwell's first equation becomes

$$\nabla \times \mathbf{H} = \epsilon''\omega\mathbf{E} + i\epsilon'\omega\mathbf{E} \quad (20)$$

The first term on the right side of Equation (20) represents the conduction current ( $I_C$ ) flow induced in the media ( $I_C = \epsilon''\omega E$  ohms law). We see that the electrical conductivity is given by

$$\sigma = \epsilon''\omega \quad (21)$$

The electrical conductivity ( $\sigma$ ) of sedimentary rocks has been measured in our laboratory and shows the first-order dependence on frequency as shown in Figure 10.

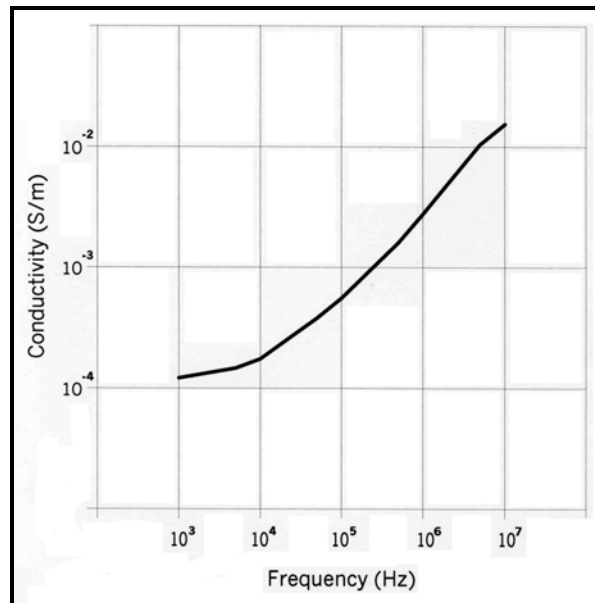


**Figure 10.** Electrical conductivity in Siemens per meter versus frequency

Due to the complex nature of the natural media dielectric constant, the electrical conductivity is frequency-dependent. The second term represents the electrical charge displacement current flowing in the media, the so-called capacitor effect due to the dielectric constant of the media. The loss tangent  $\sigma/\omega\epsilon$  is the ratio of conduction to displacement current. At the microwave frequencies, displacement current will exceed the conduction current. The electrical parameters of most natural media are frequency-dependent. This fact causes the natural media to be dispersive, which means that energy travel velocity varies with frequency. In coal, the face and butt cleat structure causes the dielectric constant to be anisotropic and represented by

$$\epsilon = \epsilon_x \mathbf{a}_x + \epsilon_y \mathbf{a}_y + \epsilon_z \mathbf{a}_z \quad (22)$$

where  $\mathbf{a}_x$ ,  $\mathbf{a}_y$ ,  $\mathbf{a}_z$  are unit vectors.

The dielectric constant and permeability of coal vary with the rank of coal and burial depth of the coal deposit (13). Figure 11 illustrates the anisotropic permeability and dielectric constant of coal.

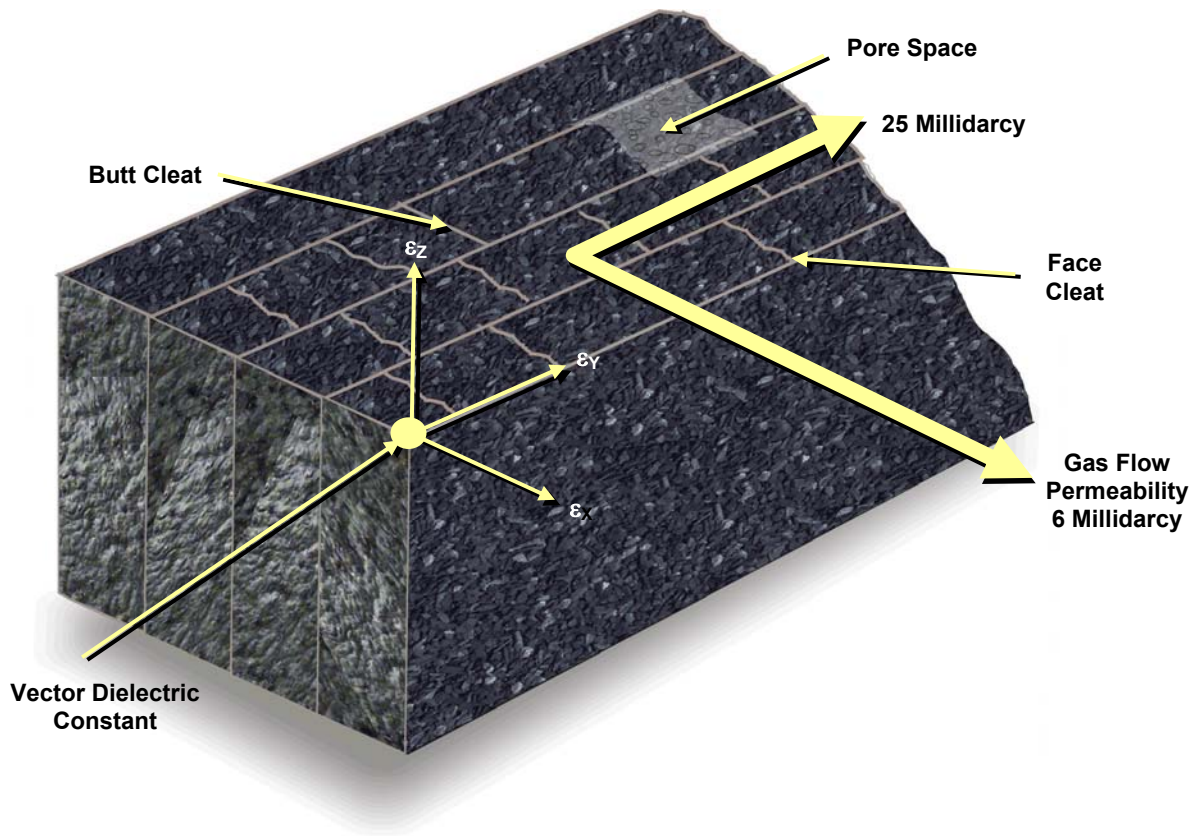


**Figure 11.** Anisotropic gas flow permeability and dielectric ( $\epsilon$ ) constant of coal

Typical permeability values are 6 millidarcys orthogonal to the face cleats and 25 millidarcys orthogonal to the butt cleats.

The anisotropic dielectric constant of coal has been observed by Balanis (14) when he was a professor at West Virginia University. The anisotropic dielectric constant causes a traveling EM wave to change polarization in abruptly changing stress fields associated with high-pressure gas outburst zones. Water-filled cleats will also change polarization. Gas well casing can be detected with vertical polarization. The cross-polarization phenomena can be measured with the instrumentation and should be developed to provide additional information for mining purposes.

## Radar Instrumentation

Radar (Radio-wave Detection and Ranging) instrumentation was developed during World War II to detect and track aircraft. Radar implies that transmitting and receiving antennas are collocated and operate as reflected (scattered) wave measuring instruments (15). These radar instruments solved the secondary field measuring (detection) problem by transmitted short-duration primary EM waves that traveled in free space at the constant speed of light ( $C$ ) and then illuminated the target at a distance ( $d$ ). The target reflects the secondary EM fields back to the radar after the round-trip travel delay time ( $t_0$ ). The time dependence of the primary and reflected secondary radar waveform is illustrated in Figure 12.

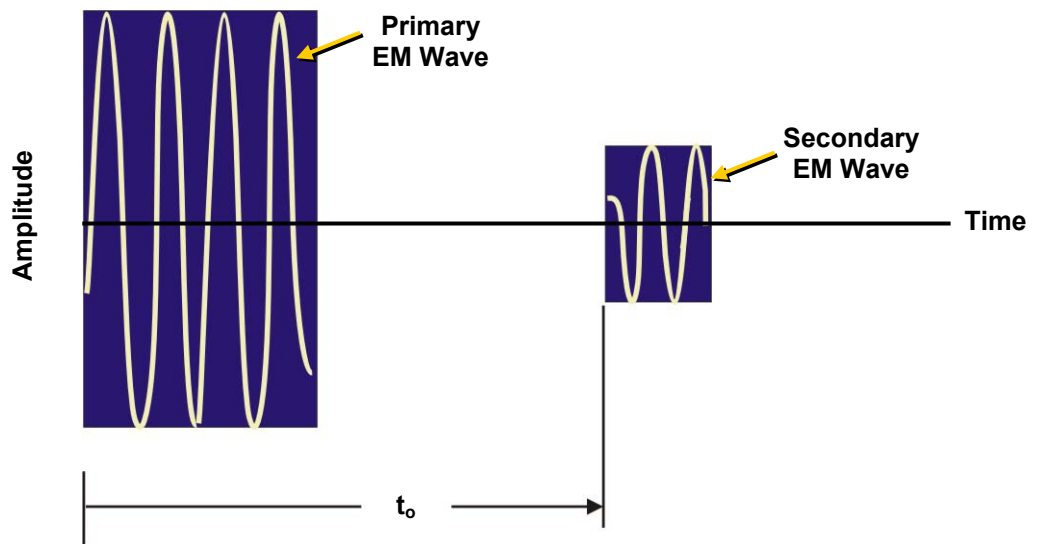


**Figure 12.** Short-duration pulse radar waveform

The radar instrumentation measures the round-trip travel time ( $t_0$ ) and a rotating antenna determined the azimuth angle to the target. The travel distance to the target being tracked is given by

$$d_0 = \frac{C}{2 t_0} . \quad (23)$$

The design of radar instrumentation encountered the practical problem of the high-energy primary wave leakage into the nearby receiving antenna. The high-energy leakage caused the

receiving antenna and the associated electronic circuits to exhibit an impulse response. These circuits ring down as the transmitter leakage energy dissipates in the circuit. Because the sensitive radar receiver can be damaged during the ring-down time period, the receiver is switched off for a short duration of time during and following each transmission burst. This causes radar to be blinded for short distance from the radar antenna location (within the near field given by  $\lambda/2\pi$ ). The far-field distance limitation occurs when the radar return (secondary EM wave) amplitude falls below the receiver inherent electrical noise. The receiver electrical noise ( $e_N$ ) is given by

$$e_N^2 = 4KTR BW \quad (24)$$

where  $T$  = the temperature in Kelvin,

$K$  = the Boltzman's constant,

$R$  = the equivalent resistance of the receiver circuit,

and  $BW$  = the noise bandwidth in Hertz of the receiver design.

The impulse radar transmitted EM wave exhibits a significant occupied bandwidth (BW). It is not uncommon for impulse radars to have occupied bandwidth greater than 25 MHz. The large occupied bandwidth and the dispersive nature of natural media are formidable problems for short-duration pulse radar applications in natural media. The large occupied bandwidth deteriorates maximum receiver sensitivity by the degradation factor

$$\Delta_{\max} = 20 \text{ Log}_{10} (BW)^{1/2} \text{ in decibels.} \quad (25)$$

The penalty paid in loss of sensitivity in a short-pulse duration radar is approximately 74 dB when compared to 1-Hz BW stepped-frequency radar receiver.

From communications theory, the optimum receiver design that maximizes the receiver sensitivity for a sinusoidal signal embedded in electrical noise is a synchronized (autocorrelation) detector (16). The synchronized receiver design drives the noise bandwidth to less than 1 Hz. It has been argued that digital sampling of the radar secondary reflected signal and digital signal processing by averaging can achieve the same receiver threshold sensitivity. This argument fails to take into consideration the digital sample's feedthrough signal limitation.

The dispersive nature of the natural media causes the occupied bandwidth frequency components to travel at different speeds, which distorts the returning secondary EM waves.

Microwave instrumentation applies transmitting antennas that are large compared to a wavelength. These systems have been developed for shallow depth of investigation. The radar instrumentation must contend with the problem that the receiving antenna is collocated with the transmitting antenna, as illustrated in Figure 13.

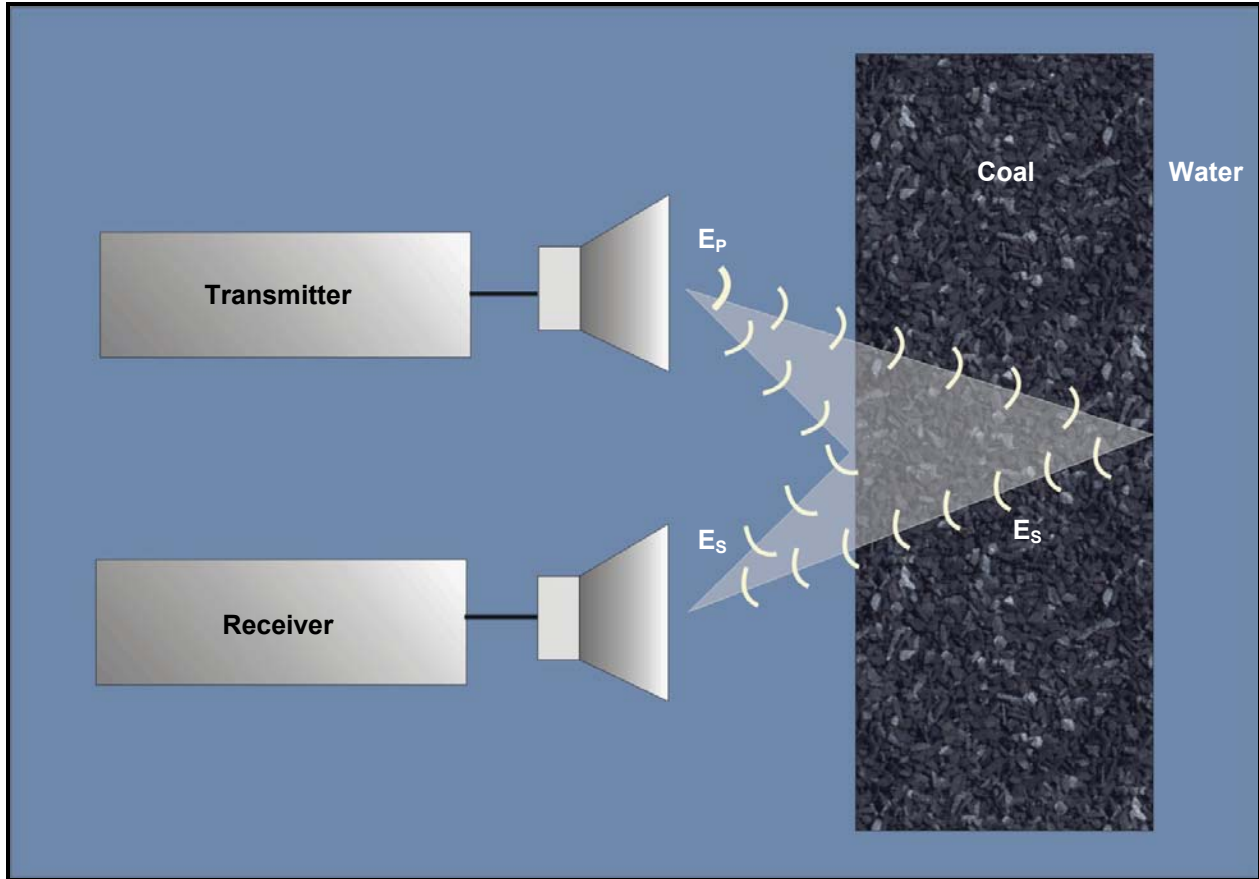


**Figure 13. Radar instrumentation**

The reflected electric field component  $E_s$  from the nearby air-coal interface can be determined from the reflection coefficient ( $\Gamma$ ) as

$$\Gamma = \frac{E_s}{E_p} = \frac{\sqrt{\epsilon_2} - \sqrt{\epsilon_1}}{\sqrt{\epsilon_2} + \sqrt{\epsilon_1}} = \frac{\sqrt{4} - \sqrt{1}}{\sqrt{4} + \sqrt{1}} = \frac{1}{3} \quad (26)$$

where  $\epsilon_2$  is the relative dielectric constant of the second media and  $\epsilon_1$  is the relative dielectric constant of the first media.

One third of the primary electric field ( $E_p$ ) is returned to the receiving antenna. The secondary electric field is only

$$20 \text{ Log}_{10} 1/3 = -9.5 \text{ dB} \quad (27)$$

below the primary electric field at the receiving antenna location. The secondary electric field reflected from the coal-water interface is only 7/11 of the primary electric field illuminating the coal-water interface. Coal-water interface reflected wave is itself reflected at the coal-air

boundary and reduced in magnitude by one-third. The secondary electric field from the coal-water interface is

$$20 \text{ Log } \frac{2}{3} \times \frac{7}{11} \times \frac{2}{3} = -10.9 \text{ dB} \quad (28)$$

below the primary wave. Thus, the reflected wave from the air-coal interface predominates the reflected wave from the coal-water interface. The radar instruments must be designed to measure the much smaller secondary field in the presence of the larger primary field.

Because of space limitations, directional couplers have been developed to allow a single microwave antenna to transmit and receive radar EM waves. Figure 14 is a block diagram of a radar designed with a directional coupler.

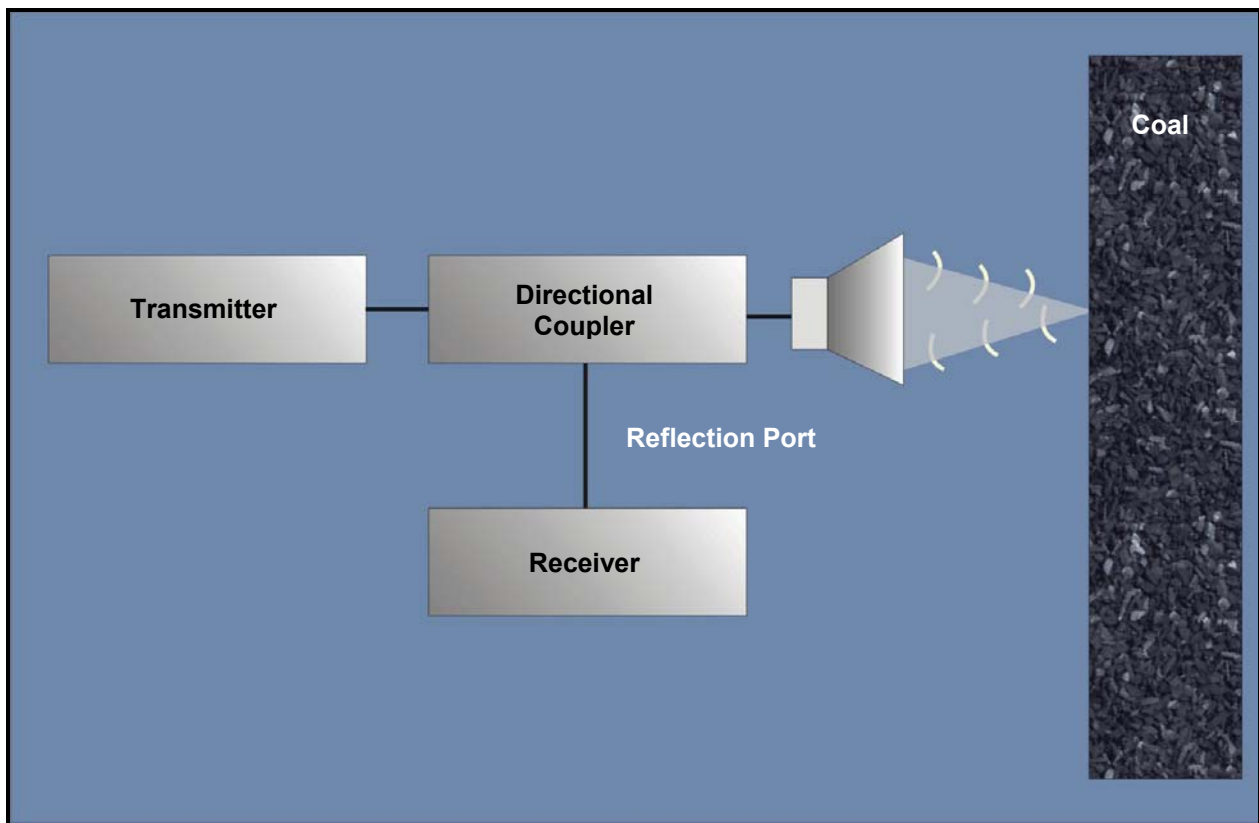


**Figure 14.** Radar with a directional coupler

The secondary reflected signal traveling toward the radar appears at the reflection port of the directional coupler. The receiver measures the reflected signal from the air-coal and coal-water interfaces. Directional couplers have a directivity limitation that is the leakage of the transmitter signal into the reflection port. Well-designed directional couplers exhibit a directivity of 100 dB, which is achieved with calibration algorithms.

The void secondary electric field from the coal-water interface is 16.5 dB below the primary wave. The electric fields traveling through the coal to the void and then traveling from the void to the radar antenna would be attenuated according to Figure 9. For a 100-dB directivity coupler, the available path attenuation limitation is

$$A = 100 - 10.9 = 89.1 \text{ dB.} \tag{29}$$

If the average coal attenuation rate is 2 dB per ft (the highest for US coal), the detection range is at least 20 ft. In the early 1970s, Cook (17) made radar range measurements in coal mines and reported the results shown in Table 1.

**Table 1.**  
**Probing distance (detection range) of a radar with a 100-dB dynamic range for coal exploration at 100 MHz**

Location	Probing Distance (ft)
Pittsburgh Seam, USA	72
Virginia, USA	66
Colorado, USA	57
Ohio, USA	33
England	23

The frequency domain radar overcomes the dispersive nature of natural media because the total phase shift at each frequency is measured by the radar phase-synchronized instrumentation. Since a time-domain pulse can be represented by a set of individual sine waves, the frequency domain radar sequentially generates each individual frequency component as a sinusoidal waveform signal to form the synthetic short-duration pulse waveform (18). The number of individual frequencies or steps required to reproduce the time-domain radar pulse depends on the resolution needed in the range-to-target detection. For the class of radar required in void detection, 50 steps are sufficient. The Continuous Wave Stepped Frequency (CWSF) radar frequency component is transmitted (remains on) during the ring down and the following measuring time periods, typically a few microseconds. Yet another important feature of the CWSF frequency domain radar is that synchronous (auto correlation) detection can be used to receive very small reflected signals. This capability increases the operating range and resolution compared to time-domain radar. The CWSF radar with synchronous detection can also be calibrated to make accurate reflected wave magnitude and phase shift measurements. The large dynamic range enables signal processing to locate voids in the coal bed. The phase-coherent synchronous detection of the radar electronics design enables gradational bed boundaries to be detected. Gradational bed boundaries will absorb a part of the forward-traveling radar signal, causing the reflected wave to be smaller than would otherwise be reflected from a high contrast (i.e., sharp) boundary.

The CWSF radar requires the measured frequency domain data to be transformed to the time domain. The Fast Fourier Transform (FFT) is used to determine the time-domain waveform. The transform is achieved in the digital signal processor (DSP) that receives input from the radar electronics. The FFT provides data for another algorithm for determining the distance from the drillhole to the boundary of the coal seam. This algorithm uses an adaptive decision method to

determine the round trip time to each reflector (i.e., boundary). To compute the distance to the reflector boundary requires the radar to measure the dielectric constant and then correct the travel time for the dielectric constant.

## Electromagnetic Fields in the Coal Seam

A natural coal seam waveguide occurs in layered sedimentary geology because the electrical conductivity of shale, mudstone, and fire clay ranges between 0.01 and 0.1 Siemens per meter (S/m) (100 and 10 ohm-meters). The conductivity of coal is near 0.0005 S/m (2,000 ohm-meters). The 10-to-1 contrast in conductivity causes a waveguide to form and waves to travel within the coal seam. The coal seam waveguide is illustrated in Figure 15.

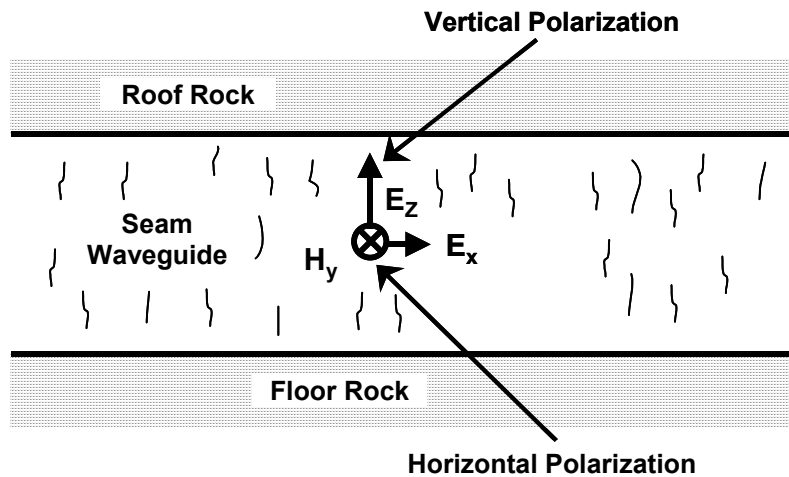


**Figure 15.** Natural waveguide for EM wave transmission

The electric field ( $E_z$ ) component of the traveling EM wave is polarized in vertical direction and the magnetic field ( $H_y$ ) component is polarized horizontally in the seam. The energy in this part of the EM wave travels laterally in the coal seam from a transmitter to a receiver. There is a horizontally polarized electric field ( $E_x$ ) that has zero value in the center of the seam and reaches maximum value at the sedimentary rock-coal interface. This component is responsible for transmission of the EM wave signal into the boundary rock layer. The energy in this part of the EM wave travels vertically in the coal deposit; the coal seam is a leaky waveguide. Due to this waveguide behavior, the magnitude of the coal seam radio wave decreases because of two different factors. The EM wave magnitude decreases because of the attenuation rate and cylindrical spreading of wave energy in the coal seam. The cylindrically spreading factor is mathematically given by  $\frac{1}{\sqrt{r}}$  where  $r$  is the distance from the transmitting to the receiving antenna. This factor compares with the non-waveguide far-field spherically spreading factor of  $\frac{1}{r}$ . Thus, at 100 meters, the magnitude of the EM wave within the coal seam decreases by a factor of only 10 in the waveguide and by a factor of 100 in an unbounded media. An advantage of the seam waveguide is greater travel distance; another is that the traveling EM wave predominantly remains within the coal seam waveguide (coal bed).

A coal seam EM wave is very sensitive to changes in the waveguide geology. The radio-wave attenuation rate (i.e., decibels per 100 ft) and phase shift (i.e., electrical degrees per 100 ft) were determined by Dr. David Hill (19) at the National Institute of Standards and Technology (NIST). Dr. James Wait (9) was the first to recognize that natural waveguides exist in the Earth's crust. Both researchers are Fellows of the Institute of Electrical and Electronics Engineers, Inc. (IEEE). The science underlying the traveling of an EM wave in a coal seam waveguide is well known.

The effect of attenuation in the coal seam waveguide is to reduce the magnitude of the EM wave along the path. The waveguide signal attenuation rate versus frequency is shown in Figure 16. The coal seam attenuation rate decreases with frequency. The wavelength increases as frequency decreases and the Radio Imaging Method (RIM) has greater operating range.

The effect of changing coal seam boundary sedimentary rock on attenuation rate is shown in Figure 17. Under sandstone sedimentary rock, the attenuation rate increases because more of the RIM signal travels vertically into the boundary rock, i.e., leaks from the waveguide. If water is injected into the coal from an overlying paleochannel, then clay in the coal causes the electrical conductivity and attenuation rate/phase shift to increase.

The attenuation rate/phase shift rapidly increases with decreasing seam height. The coal seam thinning can be easily detected with RIM. The graphical presentation of coal seam waveguide attenuation and phase constants in Figure 18 represents the science factor in the art and science of interpreting RIM tomographic images. Higher attenuation rate zones suggest that the coal seam boundary rock is changing, the seam is rapidly thinning, and/or water has been injected into the coal seam.

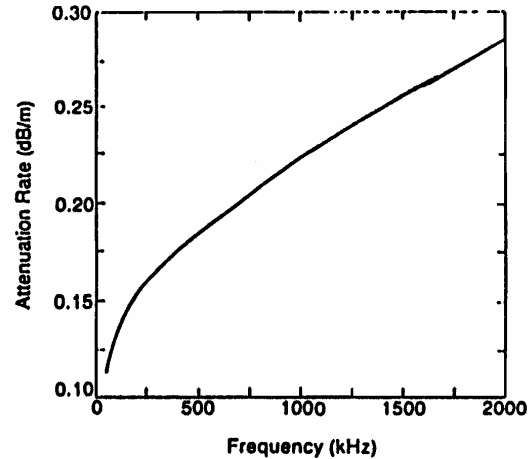


**Figure 16.** Coal seam EM wave attenuation rate versus frequency

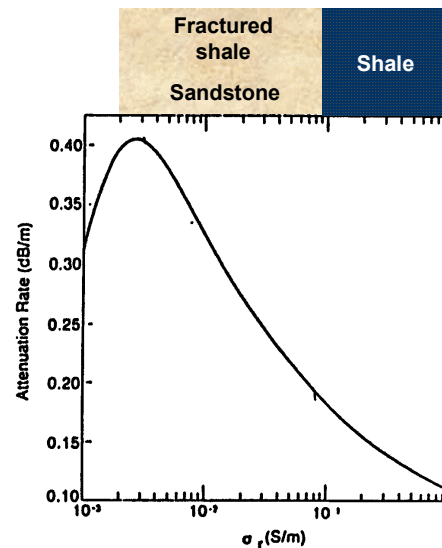


**Figure 17.** Coal seam EM wave attenuation rate versus boundary rock conductivity

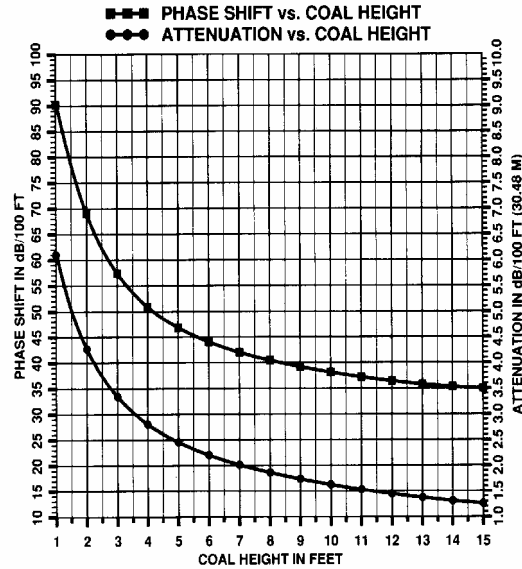


**Figure 18.** Sensitivity of radio waves to changes in coal layer thickness

Faults and dykes cause reflections to occur in the waveguide. The reflections can appear as excess path loss. Total phase shift measurements are useful in detecting reflection anomalies.

### **Coal Seam Vision with the Radio Imaging Method (RIM)**

The coal seam waveguide is effective in the frequency range above 10 kHz to at least 500 kHz. Near the low-frequency limit, in-mine experiments suggest that it is difficult to excite the seam transmission mode with reasonable size loop (magnetic dipole) antennas. At the high-frequency limit, the attenuation rate of the wave increases and limits the operating range.

Mr. Roger Fry, Senior Geologist at Utah Power and Light Company, and Stephen Doe, Senior Geologist at American Electric Power’s Meigs Division mining complex, undertook the first RIM tomography surveys in 1985 and 1986 (20–23). Since then, RIM has been used extensively in the United States, Australia, New Zealand, South Africa, and the United Kingdom to evaluate coal seam geology (24, 25). More than 500 surveys have been conducted world wide.

RIM has proven cost effective in detecting voids and geologic anomalies in coal beds. RIM EM waves strongly interact with the types of geologic anomalies shown in Figure 19. The observable in the RIM data is increased attenuation rate.

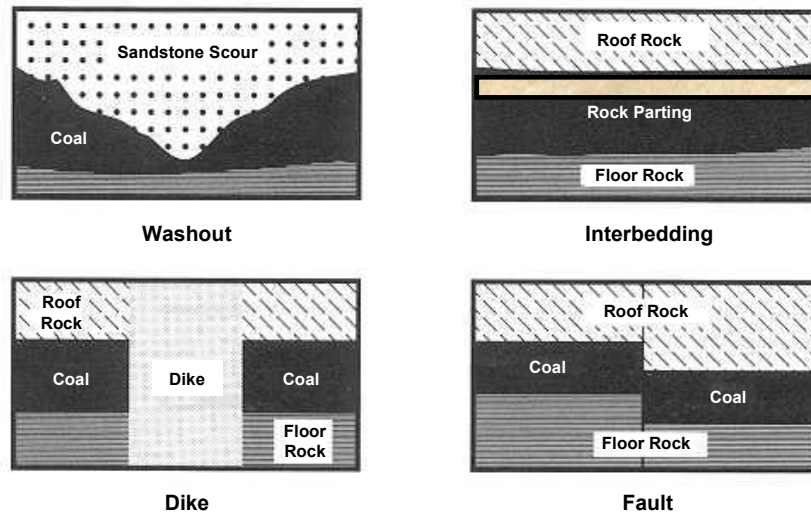


**Figure 19. Natural coal seam anomalies**

Mine safety is adversely impacted near anomalous geologic zones. Dikes, faults, and paleochannels alter the roof rock and contribute to the potential for roof falls. Oftentimes, high-pressure water and gas are trapped in slip fault zones. Rock falls occur along the margins of paleochannels as illustrated in Figure 20.

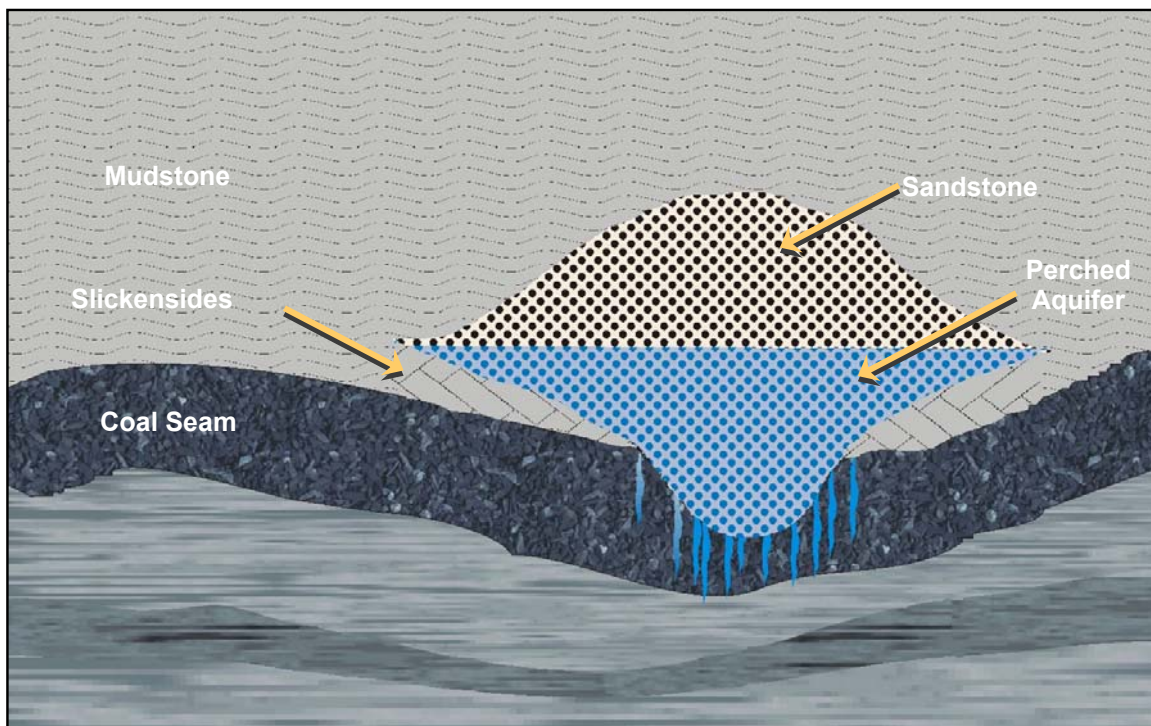


**Figure 20. Cross section of a paleochannel**

Differential compaction combined with scouring and thinning of sedimentary rock overlying the seam creates the roof fall hazard. Roof control should be more aggressive in entries that are developed under channel margins.

Dealing with the problem of minimizing mining hazards and risk involves a three-step procedure: detection, confirmation, and mitigation. RIM is cost effective in detection of voids and geologic anomalies. Confirmation requires two steps. First, tomography surveys provide a silhouette map of the anomalous region and higher attenuation rate zones locate voids and anomalies. Second, using tomography as a means of targeting, horizontal directional drills with integrated radar can acquire confirmation data. Mitigation may require accurate horizon control of the cutter drum under the channel margins.

Tomography resolution has been improved with the development of three-dimensional (3-D) processing algorithms. The comparison of tomography algorithms is illustrated in Figure 21.

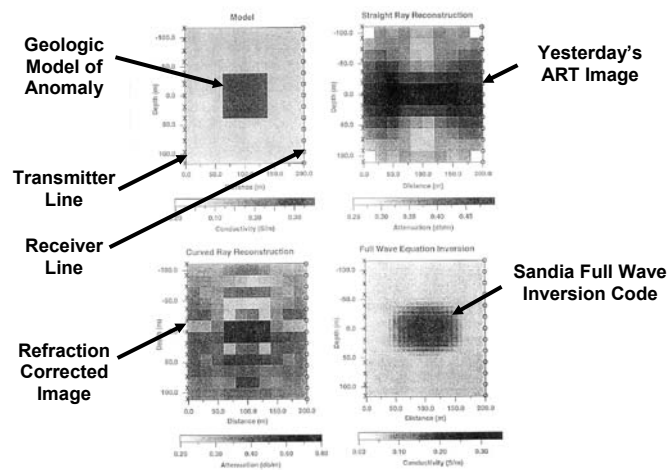


**Figure 21.** Comparison of RIM image reconstruction methods

The comparison of reconstructed images shows that the algebraic reconstruction technique (ART) produces a smeared image in the direction of wave propagation. The ART algorithm assumes that the coal seam waveguide signal travels on a straight ray path. Severe geologic anomalies cause refraction of the signal, and the ray path assumption fails. This is the cause of the smeared image. In mild anomalies in the Pittsburgh coal seam, the image is not significantly distorted. Cross-panel RIM tomography has proven effective in detecting geologic anomalies within longwall panels. The full-wave algorithm processes the RIM receiver magnitude and phase data to reconstruct the image with much higher resolution than ART.

Advanced RIM instrumentation has been developed that achieves an operating range exceeding 1800 ft in coal beds (26).

The instrumentation was applied in the detection and imaging of dykes, faults, and paleochannels. The image of a paleochannel in a longwall panel is illustrated in Figure 22 (26).

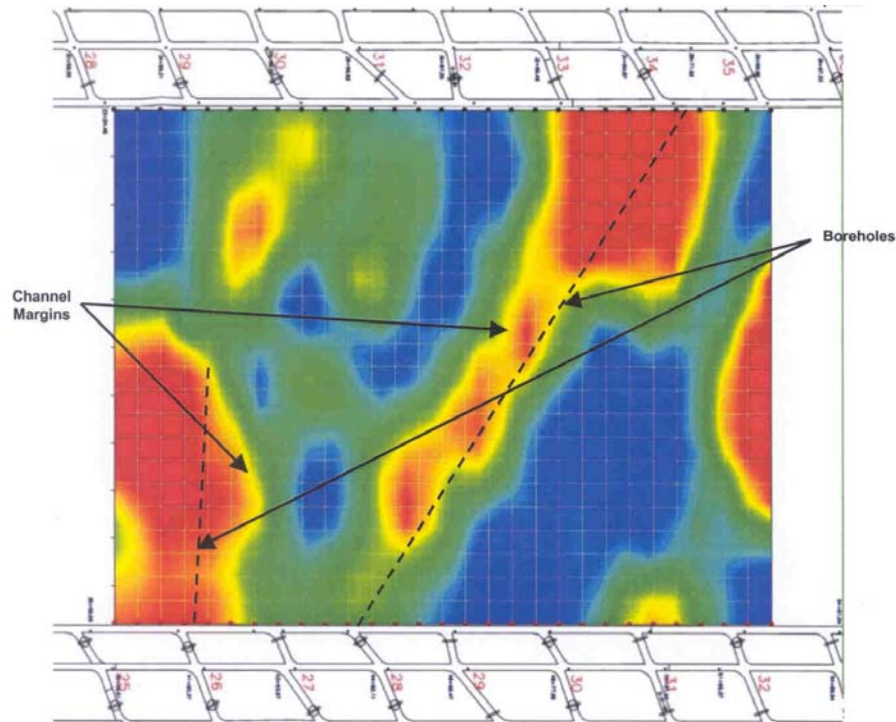


**Figure 22.** Image of a paleochannel in a 1,000-ft-wide longwall panel

The image maps the attenuation rate of the RIM-IV signal in the coal bed. The warmer colors indicate the regions of the panel where the attenuation rate increases; geologic anomalies are suspected within the red zone. Since the RIM-IV signal attenuation rate increases under a paleochannel, the red zones illustrate paleochannels crossing the longwall panel. Oftentimes, meandering channels scour into the coal bed where the energy of the water flow is maximized (cut bank). Along the margins of the channel, the roof rock is fractured by differential compaction. It is not possible to determine the amount of scouring or roof rock fracturing from the image alone. Mine planning requires an additional step of confirmation. Confirmation can be achieved by horizontal directional drilling (dashed line) in the red zones to determine seam height. Oftentimes, undulations in the coal bed occur under a paleochannel. However, horizontal drilling requires improved guidance and navigation technology to ensure the drill stays within the seam and intersects the target. By integrating radar and navigation technologies (such as drillstring radar [DSR]) with horizontal drilling, the seam height can be mapped along the drillhole, and this feature will ensure adequate guidance. The coal bed undulation can be determined from the processed radar data and navigation information used to enable accurate confirmation.

Crosswell RIM-IV instrumentation can complement directional drilling by imaging between pairs of boreholes. Tomographic imaging can map voids between two parallel boreholes or between a mine entry and a horizontal borehole. Tomographic imaging requires the movement of the RIM-IV receiver and transmitter in the boreholes. The transmitter can be maneuvered with the horizontal drilling machine.

## **Void Detection with Electromagnetic Wave Methods**

Pennsylvania Governor Mark Schweiker’s special Commission on Abandoned Mine Voids and Mine Safety Report recommendation for detection and imaging technologies is achieved by integrating radar on horizontal drills and applying RIM crosswell imaging. Over the past 20 years, there have been a total of 449 inundations in underground mines—397 in coal and 52 in metal/non-metal mines (27). These inundations have occurred at the rate of nearly two per month. To decrease the risk of mining into old works, mines operating within 200 ft of a known working are required to drill boreholes 20 ft in advance and at 45-degree angles every 8 ft of development. The combination of radar and RIM is cost effective in that drilling every 8 ft of advance increases product cost by as much as \$5 per ton.

### **Stolar Radio Imaging Method in Void Detection**

#### **3-D RIM to Locate and Image Mine Voids**

Several configurations of RIM instrumentation are available for deployment at the mine site for void detection surveys. These configurations consist of an in-mine man-portable RIM system for use in exiting entries, and a borehole probe system for use in drillholes originating from either the surface (vertical boreholes) or in-seam (horizontal boreholes). The systems are flexible to enable combinations of borehole to in-mine scans as well.

The RIM technology can be used to help current mining operations avoid old mine workings by two methodologies: (1) confirmation of barrier pillar integrity with a pillar fence line, or (2) location and imaging of the old workings with tomographic imaging.

## **Principles of Void Detection with RIM**

Irrespective of which survey method is used (fence-line or tomography), the detection of voids (mine entries) within a coal seam using RIM is based entirely on the waveguide behavior of the coal seam itself. The RIM EM wave travels in a “trapped” mode in the coal between the conductive roof and floor material. The EM wave travels along a “ray path” or “wave front” from transmitter to a companion receiver, decaying in signal strength as a function of distance. In homogeneous conditions, the rate of this decay is consistent and predictable beyond the near field of the transmitting antenna.

In a homogeneous coal seam, the EM wave (radio signal) attenuates (decays) with distance traveled at a fixed rate; this is termed the attenuation rate. If a geological anomaly exists along the ray path, the receiving antenna will measure lower signal strength (increased attenuation rate). Geological anomalies that will affect the RIM signal include faults, dykes, paleochannels, seam thinning, and increased water in the seam. Non-geological anomalies that may affect the RIM signal include abandoned mine works. If a portion of that seam waveguide is water-filled or air-filled, the rate of decay changes. A plot showing the normal attenuation rates (as a function of frequency) in air, coal, and water is shown in Figure 23.

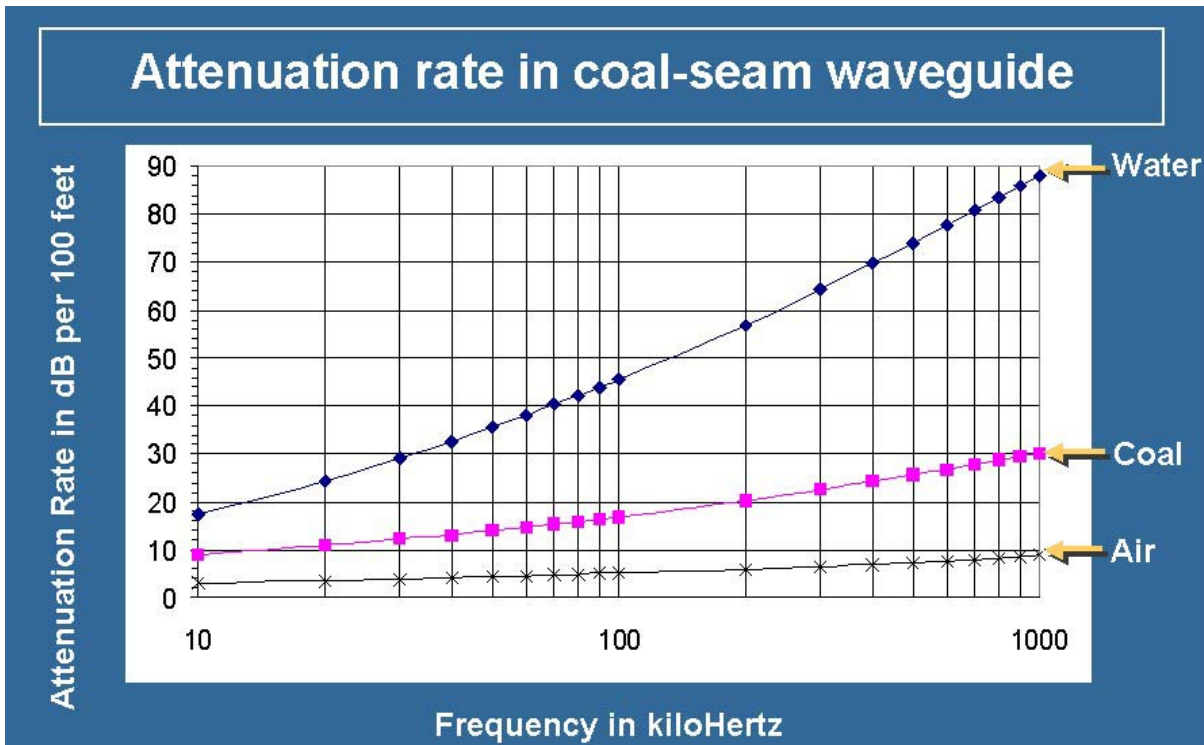


**Figure 23.** Normal attenuation rates (as a function of radio-wave frequency) for water-filled, air-filled, and coal waveguides

As an example: if a 100-kHz radio wave travels 100 ft in a coal seam with a normal attenuation rate of 18 dB/100 ft, it decays by 18 dB. If the radio wave must travel through a 20-ft-wide water-filled entry, it will decay at a rate of 45 dB/100 ft over those 20 ft instead of the coal-based rate. The difference between the coal rate and the water rate is 27 dB/100 ft and its effect on the attenuation is an additional 5.4 dB (excess loss = 20 ft x (0.45 – 0.18) dB/ft = 5.4 dB). Therefore, the total signal loss for the radio wave is 23.4 dB instead of 18 dB due to the presence of the water-filled entry (a 30% increase for a 100-ft signal path).

The example described above is an idealized case. The attenuation rates measured in the field are a function of seam thickness, geology, electrical conductivity, and moisture. Most coal seams have a standard attenuation rate of 5 to 10 dB/100 ft, which increases 3 to 6 dB if entries are encountered.

### 3-D RIM Configurations

The RIM instrumentation systems currently available for field use are in-mine and downhole instrumentation.

#### In-Mine 3-D RIM Survey Instrumentation

The in-mine instrumentation is illustrated in Figure 24. The synchronizing (sync) signal is sent from the sync transmitter through the coal seam waveguide to a companion receiver at a very low frequency. Figure 9 shows that the low-frequency sync signal is insensitive to the geology of the coal bed. The sync is recovered at the sync receiver and then sent over non-conducting fiber-optic cable to the RIM-IV receiver.

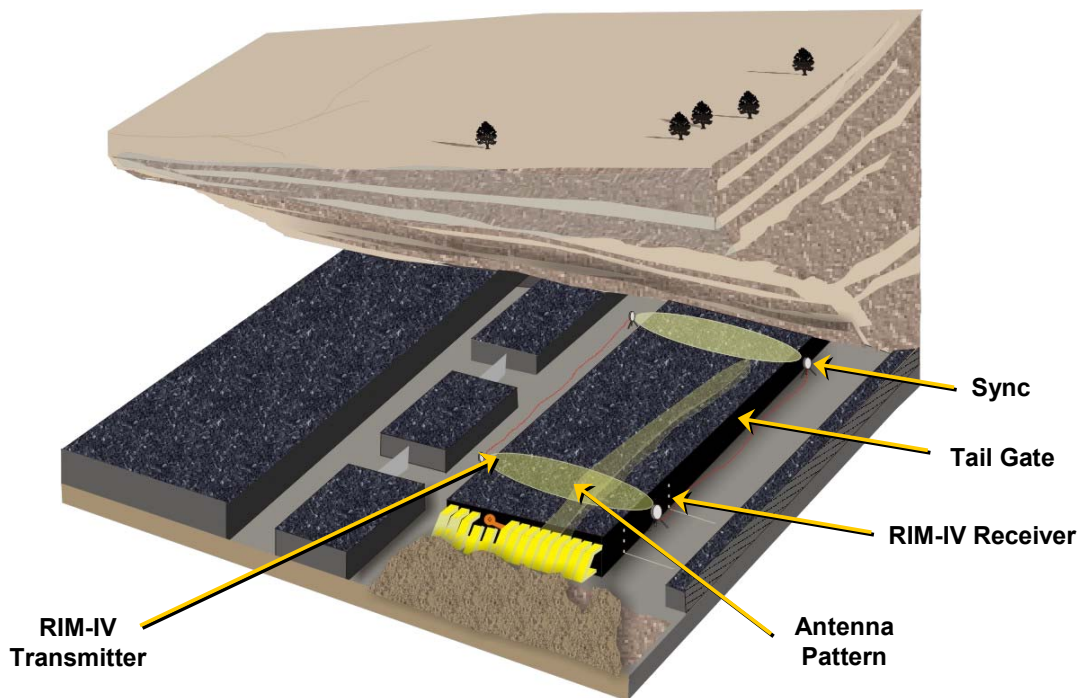


*Figure 24. In-mine instrumentation*

The in-mine system incorporates environmentally sealed housings for its electronics or antennas and is awaiting final assembly in flameproof and sealed enclosures for its electronics, battery pack, and antennas. The in-mine 3-D RIM instrumentation consists of a transmitter (TX) and a receiver (RX). The current In-Mine RIM transmitter instrument is shown in Figure 25.



**Figure 25.** In-Mine RIM-IV transmitter

Fiber-optic cable and adapters interconnect the In-Mine 3-D RIM instruments to air-core loop antennas (hermetically sealed) and a central graphical user interface (GUI) housed in an explosion-proof (X/P) enclosure.

### **Downhole Survey Equipment**

The downhole RIM-IV instrumentation can be applied in vertical boreholes as illustrated in Figure 26.

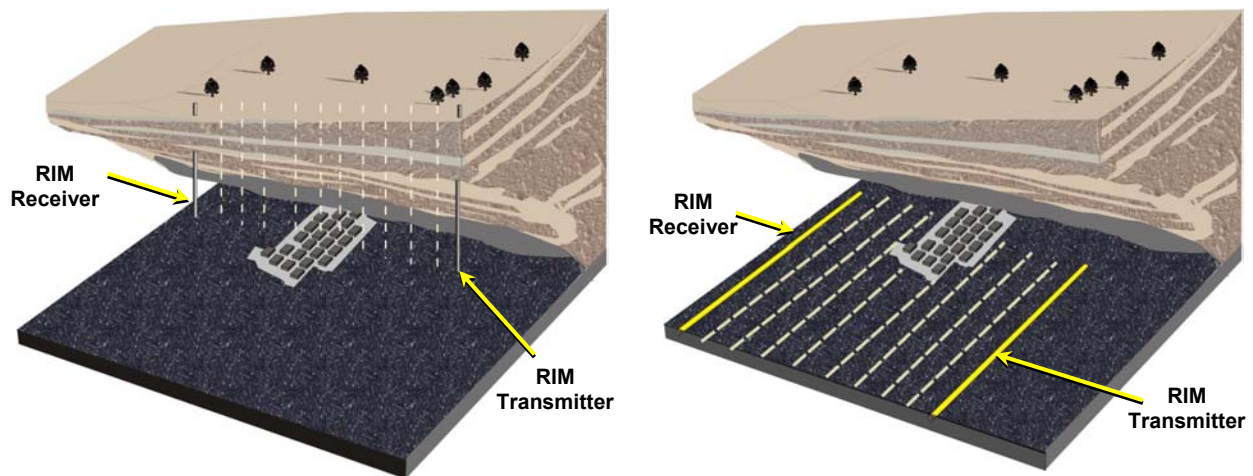


**Figure 26.** Crosswell RIM-IV reduces drilling cost

The RIM downhole instrumentation consists of a multi-frequency transmitter and receiver units designed for borehole applications. The antennas consist of wound ferrite cores powered by downhole batteries and phase linked by a fiber-optic synchronization cable. The field procedure

is to set up transmitter (TX) and receiver (RX) units in adjacent boreholes and measure the decay of the RIM signal over distance (the “measured signal strength”). Signal strength will be diminished by any disruption to the seam waveguide properties—in this case, by voids associated with underground mine works. Figure 27 illustrates void detection with RIM crosswell instrumentation.

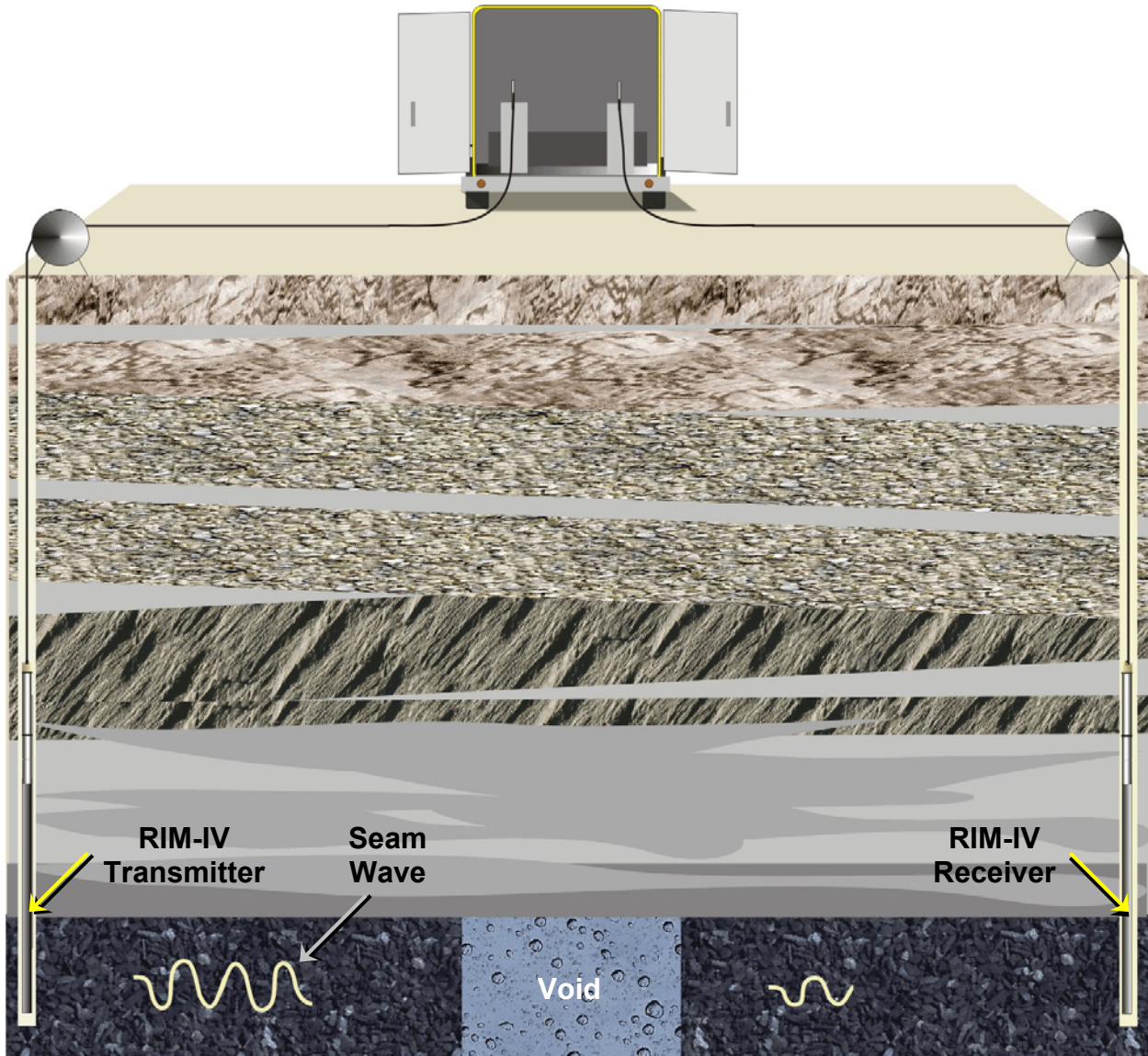


**Figure 27.** Crosswell detection of a coal seam void

The survey involves the use of a central control unit (instrumentation trailer) that houses the TX and RX hoists and a data logger/computer. Field personnel communicate by means of two-way radios to synchronize the insertion of the probes into the borehole, the lowering of the antennas to the appropriate horizon, and the removal of the probes from the hole. Coordination of the project is the responsibility of the senior RIM engineer located in the central control unit.

The data are recorded on computer and subsequently downloaded and interpreted by a qualified Stolar geophysicist. The Stolar RIM Instrumentation Trailer is shown in Figure 28. The RIM Trailer can be placed anywhere in the borehole pattern and sequentially deploy its downhole probes over fiber-optic cables to the borings.



**Figure 28.** The RIM downhole probes are lowered into vertical borings using fiber-optic cable (left photo). Stolar's RIM Instrumentation Trailer contains two (2) cable hoists, control electronics, and probe inventory (right photo).

The antennas are lowered to the middle of the seam in both TX and RX boreholes, and the signal propagates through the coal seam waveguide. The RX unit measures the signal strength. It is important to have available accurate seam depth information in order to position the antennas in the appropriate part of the coal sequence. However, irrespective of the provided depth information, experimentation in the field by the RIM engineer will confirm the position of the antenna in the seam (moving of the probes out of the coal will result in a noticeable decrease in signal strength).

The advanced downhole 3-D RIM is shown in Figure 29. This packaging includes stainless steel or titanium X/P housings for all the electronics and batteries. The antenna housing is a fiberglass composite and the mil-spec fiber-optic cable is deployed from a portable electric hoist.



**Figure 29.** Receiver probe for the Downhole RIM-IV system deployed for field-testing

The current design of all Downhole 3-D RIM systems includes Intrinsically Safe (I/S) and X/P components for in-mine and in-seam use. The I/S components include the antenna assemblies (TX and RX) and the battery packs. The X/P components are housed in X/P enclosures and include the fiber-optic adapters and the electronics (TX and RX). Downhole 3-D RIM uses ferrite-core loop antennas (hermetically sealed) and a central GUI housed in a non-X/P enclosure for surface use.

### **Phase Synchronization**

The Downhole 3-D RIM design allows the TX and RX sections to be connected, via fiber optics, through to the display enclosure. This “hardwire link” allows the phase synchronization to be maintained at all times during use of the system. With synchronization, accurate measurements of signal phase shift can be made for all ray paths yielding higher signal-to-noise ratios, which is highly desirable.

The In-Mine 3-D RIM design allows for the same type of “hardwire link” to be used underground, providing the TX and RX sections can be connected via fiber optics. If this is not possible, then the cable can be replaced with a radio-link system (20 kHz) that does an effective job of maintaining phase coherence.

As indicated above, the RIM systems can be deployed in combination to provide the industry with different approaches for void detection and/or barrier pillar confirmation. The following illustrates different approaches.

## RIM Method 1: Fence-Line Confirmation of Barrier Pillar

Figure 30 shows a mine plan map adjacent to a complex of abandoned mine workings. The area of solid coal between the old works and planned works is the barrier pillar.

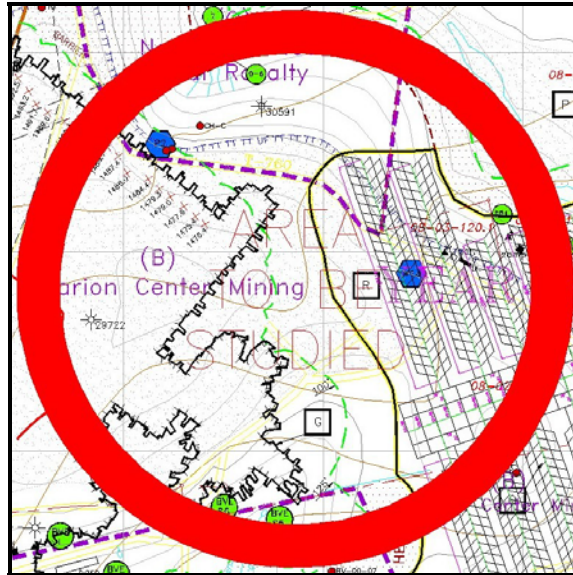


**Figure 30.** Map of a mine's target area. The old workings are the outlined structure to the left, while the new workings are shown as a projection of entry grids to the right.

Mining engineers are considering all options to confirm the boundary of the old works and/or integrity of the pillar. These options include extensive drilling using vertical and horizontal drill methods. The goal of the drilling is to verify the existence of a solid pillar between the workings (old and new) and possibly to locate water-filled voids in the coal seam that indicate the location of an abandoned mine entry.

The primary method of barrier pillar confirmation is a fence line of boreholes. The fence line consists of a series of boreholes at varying separation distances (200 to 1000 ft) that form a boundary line between the old works and the mine plan development entries. The distance from the fence line to the planned mine works is equal to the minimum distance required for a barrier pillar in the area.

For a fence line of 2000 ft, only 4 to 10 boreholes would be needed using the RIM fence-line approach. Using surface drilling alone, as many as 100 vertical boreholes, spaced 20 ft apart, would be required to confirm the integrity of the barrier pillar along the same 2000-ft boundary line (assuming the old working entries are 20 ft wide). If the average depth of the coal seam along this line is 300 ft, the cost to rotary drill 100 vertical boreholes could exceed \$300,000. The advantage of a RIM survey is that considerably fewer boreholes need to be drilled because the RIM systems can scan between holes, providing valuable information and eliminating the need for such a tight drilling pattern.

The primary technical objective of the RIM fence-line survey is to confirm whether there are water-filled (or air-filled) voids that might be the result of old works along the boundary line. The following outlines the survey plan for a fence-line survey.

### Fence-Line Survey Plan

For a 2000-ft fence line in a 6-ft thick coal seam possessing moderate attenuation rates, the approach is to form a fence line through which old workings must not pass if the barrier pillar is to maintain a safe minimum width. The position of the fence line should be the required distance from the proposed location of the new mine workings. If RIM can establish the presence of a continuous coal seam between adjacent boreholes on the fence line, then the barrier pillar is of sufficient width and seam continuity. The locations of the fence line and the RIM survey boreholes for the example mine map are shown in Figure 31. Boreholes to the right of the fence line at locations 2 and 9 can be drilled to confirm that an old works entry has not circled behind the fence.

Drilling logs of the boreholes are a helpful component in the survey planning so that the depth and thickness of the coal seam for each borehole are known. It is also critical that surface conditions (topography, vegetation, etc.) allow the routing of fiber-optic cables between adjacent boreholes.

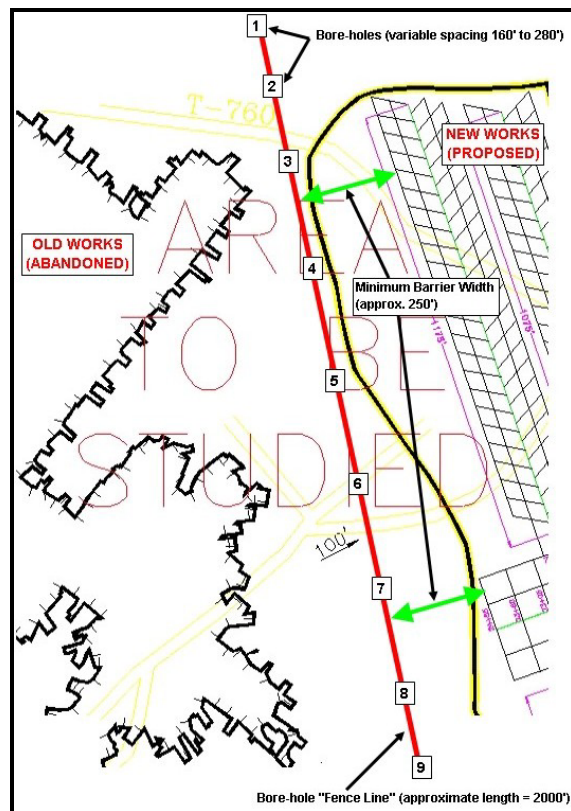


**Figure 31.** Diagram of RIM survey site showing the pillar fence line (red line) and the nine (9) proposed borehole locations (numbered boxes) relative to the old and new mine workings

### ***Calibration Survey***

The first objective of the survey is to establish the appropriate RIM antenna frequency to be utilized and the optimal resolution with which to sample the seam. This is termed the calibration survey.

The calibration survey involves deploying the RIM TX and RX probes into adjacent boreholes, lowering them to the center of the coal seam, and measuring radio-wave signal and phase for a variety of radio frequencies between 50 kHz and 500 kHz. It is desirable to use the highest frequency possible given the range requirements of the survey. Higher frequencies imply greater resolution, but the subsequent tradeoff is a decrease in the range of the instrumentation. In the target area, the calibration survey will be carried out between Boreholes 1 and 2 (minimum ray-path length), and again between Boreholes 7 and 8 (maximum ray-path length). The calibration survey will take four (4) to six (6) hours to complete.

### ***Reconnaissance Survey***

After the antenna frequency is selected, the objective is to take as many measurements as possible from the eight (8) borehole combinations in order to define the continuity of the seam; this is termed the reconnaissance survey. The reconnaissance survey involves deploying the RIM TX and RX probes into adjacent holes, lowering them to a point above the seam, and measuring radio-wave signal and phase.

Each hole-to-hole ray path, termed a “shot”, can be performed relatively quickly once the instrumentation trailer and hoists are in place and the probes are in the boreholes. The RIM crew can perform four (4) to six (6) reconnaissance shots per day dependent on surface topography, obstructions, and borehole depth.

## **RIM Method 2: Tomographic Imaging of Mine Workings**

A more involved method for using RIM in void-detection applications is the actual mapping of old workings using image-generation techniques and software. 3D-RIM is able to transmit signals through greater distances than previous RIM technologies, and the advanced system measures and detects signal phase shift. When coupled with advanced Full Wave Inversion Code (FWIC) software modeling packages, the phase-shift data produces greatly enhanced and higher-resolution tomographic and 3-D images.

High-resolution tomographic imaging of in-seam structures allows us to focus on an area and create detailed two-dimensional (2-D) and 3-D images of the survey area for the purpose of resolving the size, shape, and trend of specific geologic disturbances or structure, such as mine entries and barrier pillars. The resolution of these images is dependent on shot location and the density of the 2-D or 3-D ray paths through the area.

The primary objective of a RIM tomography survey would be to develop an image of existing old workings so that their location and extent are known for current mine planning. A sample map of old workings near a highwall outcrop is shown in Figure 32. This group of old

works originated in highwall and is approximately 2000 ft long and 600 ft deep into the highwall. A RIM image of the workings (termed a “tomogram”) could be generated at the highest resolution possible so that the shape, size, and location of the entries can be discerned within the image.

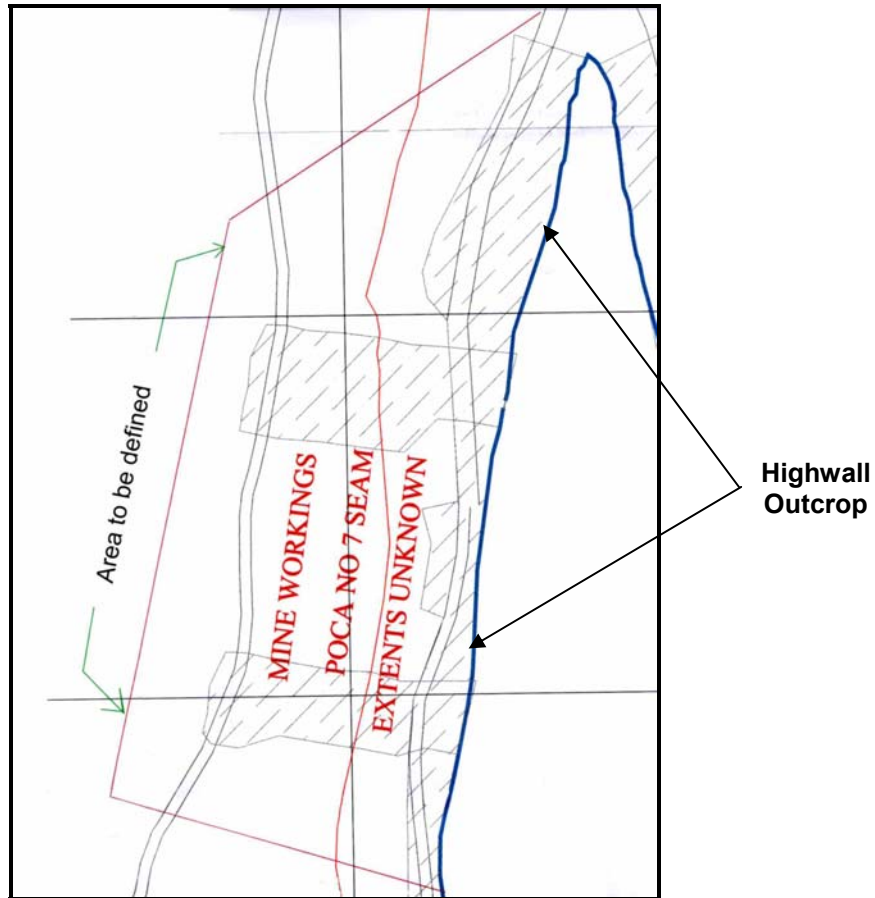


**Figure 32.** Map of the old workings originating from a highwall bench

For this application, a highwall outcrop of the coal seam will be used in conjunction with boreholes distributed throughout a 2200-ft by 800-ft area centered on the old works. Direct lines of radio frequency transmissions (ray paths) between the boreholes and the outcrop provides the RIM data necessary to define the workings. The boreholes are located at strategic locations, of variable separation, to provide optimal resolution when used with ray paths to the outcrop. The resulting image forms the approximate shape and location of the workings to accuracies within 50 ft, depending on borehole spacing.

### **RIM Tomography Survey Plan**

The RIM tomography technique provides very detailed 2-D and 3-D images of the survey area based on mathematical reconstructions of many ray-path data sets.

The ray paths required could be generated using a plan of 12 boreholes and 11 outcrop locations. The boreholes are distributed through the old works in two rows on roughly 400-ft centers. The outcrop stations are at coal seam level within the highwall pit on 200-ft centers. Using these 23 stations for radio-wave transmission and reception, there could be 81 possible ray paths to use for tomographic processing and imaging. A diagram showing the possible borehole and outcrop locations is shown in Figure 33.

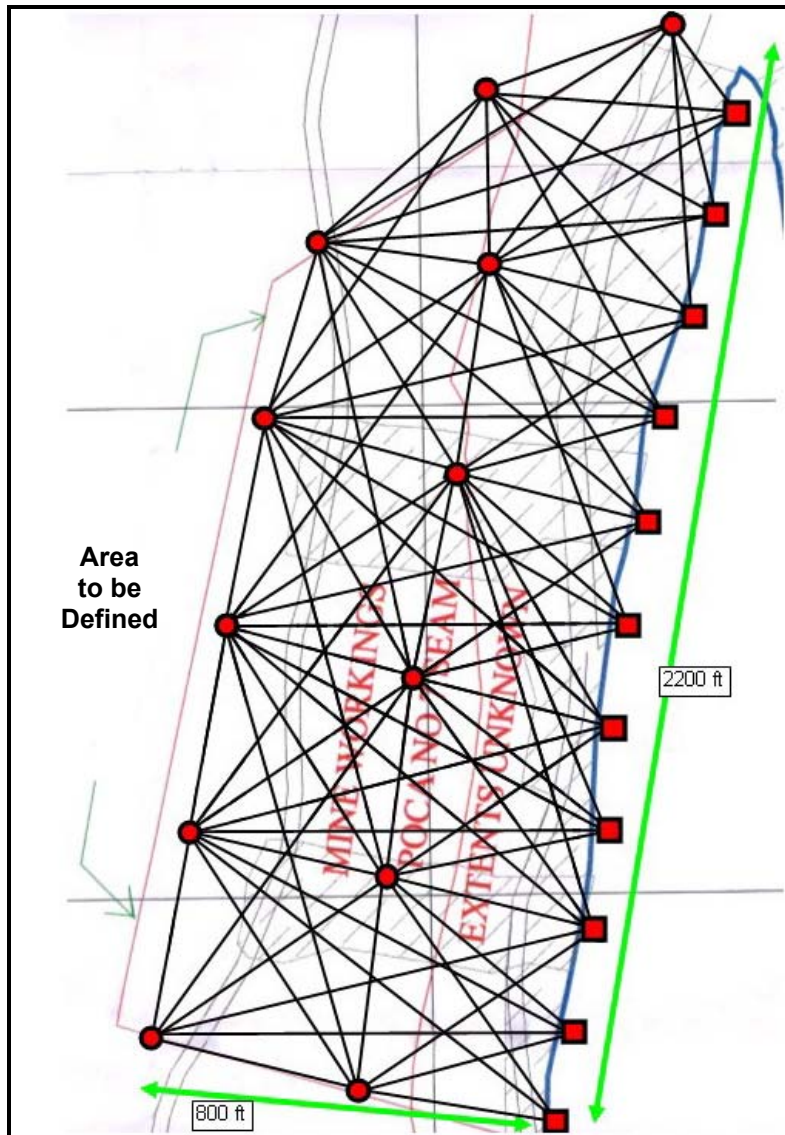


**Figure 33.** Map of a recommended survey plan at an old-workings site

The resulting tomographic image (tomogram) would consist of a plan view contour map showing the shape and location of the old workings and their entries. The locations, relative to the boreholes, could then be projected to existing surface maps and mine plans to evaluate their proximity to current or proposed workings. The number and location of boreholes can be modified based on final logistics and the required scope and scale of the imaging project.

The time required to perform the tomography survey is dependent on the number of borehole combinations used. The RIM crew can perform twenty (20) to thirty (30) tomography shots per day dependent on surface topography, obstructions, and borehole depth, therefore, the 81 ray paths proposed would take three (3) days to complete.

### RIM Tomography Survey Results

For example, a dike system penetrating a coal seam could be effectively imaged by straddling it with a borehole grid for tomographic surveying, as shown in Figure 34. The sample grid, comprised of nine (9) boreholes, would have a maximum hole-to-hole separation determined during calibration. As with the reconnaissance survey, any combination of ray paths can be adopted based on the target size, practical boring pattern, and desired resolution.

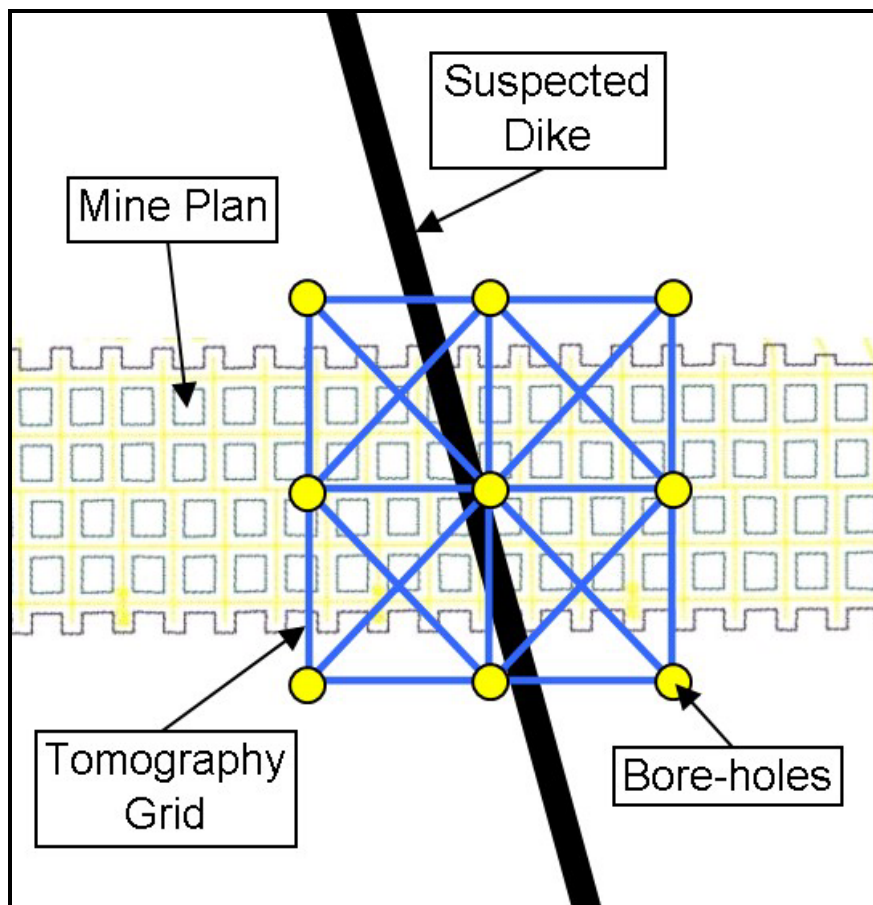


**Figure 34.** Location and borehole pattern of tomography grid over a suspected dike

A sample tomography survey image through the dike, at 1000-ft borehole separations, is shown in Figure 35. In this example, the attenuation rate of the RIM signal passing through the dike is 6 dB/100 ft higher than that through continuous coal. The location of the dike is quite evident on the plot and it is possible to estimate the dike shape, trend, and thickness. This image is at the top of the coal seam.

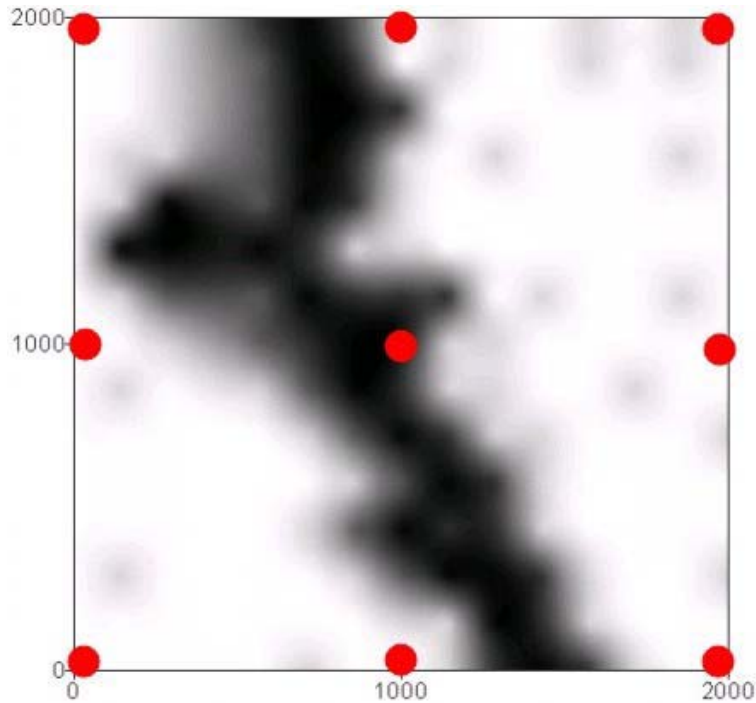


**Figure 35.** Two-dimensional images for a 2000-ft tomography survey grid over a dike at a 1000-ft hole-to-hole separation

## RIM Case Study

A RIM survey was recently conducted to investigate geological conditions and the extent of abandoned mine works ahead of proposed mine development. A mine had re-entered previously developed mine works from a highwall adit, and was extending operations down-dip into unmapped regions. Previous mine works in the area were well documented, but it was possible that some historical mine works were not shown on existing plans. In addition, the mine was affected by seam roof paleochannels that could hinder coal extraction.

The RIM survey was designed both to detect abandoned mine works and evaluate geological conditions ahead of mining. The objectives of the imaging program were to:

- Establish the location of zones of coal that may be affected by abandoned mine works
- Provide an objective evaluation of seam geological conditions ahead of mining
- Make recommendations regarding an appropriate approach to managing geological and/or old mine works risk at the mine.

## Case Study Survey Procedure

A plan of the survey site with borehole locations, a summary of borehole stratigraphic column, and a map of known historical mine works were provided prior to survey start-up. Aerial photographs of the survey site, borehole locations, a summary of borehole stratigraphic columns, and predicted location of the works are helpful in pre-survey planning.

In general, RIM equipment should be deployed into vertical boreholes lined with PVC casing, never metal casing. This prevents damage or loss to the system resulting from hole collapse or debris. If the geology is exceptionally competent, the probes can be used without PVC casing. The borehole depths can be a minimum of 20 ft and a maximum of 1500 ft.

The basic geology of the survey area, as well as coal seam geology, needs to be characterized in general terms prior to developing a survey plan. Drill history provides a good geologic picture, particularly in identifying seam position and thickness. The dominant bounding rock in the stratigraphy is important in determining optimal imaging frequency and borehole spacing. These rock types may include clay, shale, siltstone, and sandstone. It is also important to know if there is evidence of geological anomalies, such as paleochannels, faults, and dykes, in the survey area. Without this information, it must be assumed that the seam is homogeneous throughout the survey.

The survey utilized RIM equipment from vertical boreholes and from underground in-mine, hand-held units. A total of 44 individual ray paths were measured from 14 individual boreholes (ST-1 to ST-13, and MA92-12) and 9 underground survey stations. The boreholes were drilled to a maximum depth of 10 ft below the coal seam level. The survey layout of the boreholes and the current workings is shown in Figure 36. The survey was carried out using two frequencies: 242 kHz and 432 kHz. The lower frequency was used for the longer borehole-to-borehole shots; the higher frequency was used for closer borehole spacing and borehole-to-in-mine shots. In general, experience dictates that it is desirable to use the highest possible frequency in order to achieve higher resolution. Also, advanced RIM systems have synchronized signals enabling the collection of phase shift data, which when utilized with attenuation rate measurements provided a most superior analysis/image.

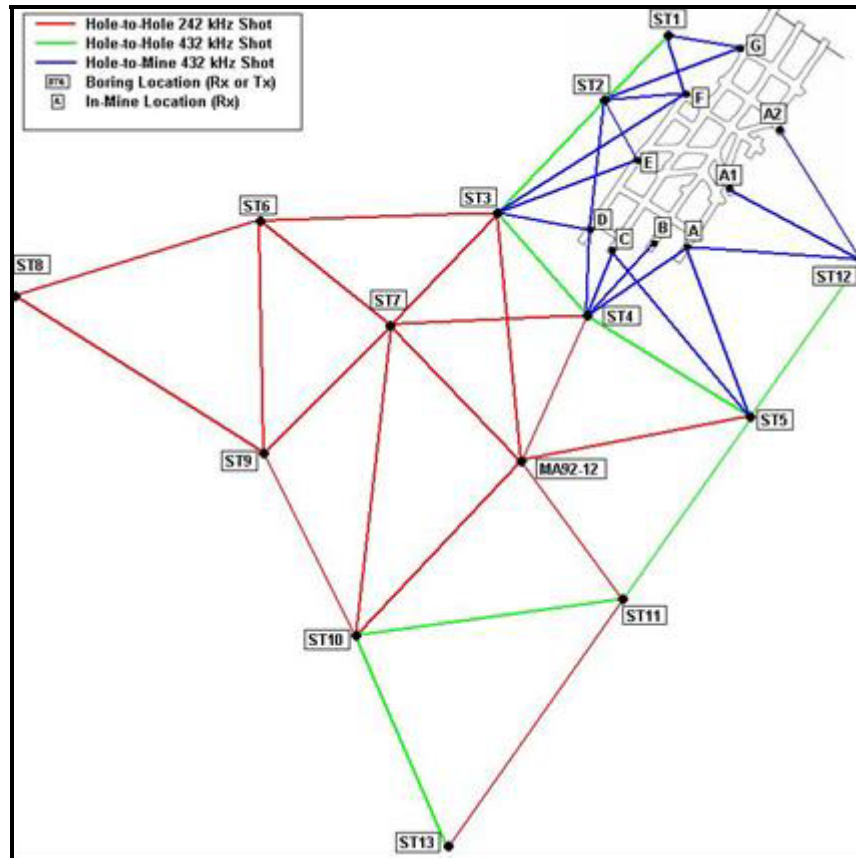


**Figure 36.** Diagram of the survey area showing downhole boring location, in-mine receiver station, and transmission ray path

## Case Study Survey Results

The establishment of a standard RIM response in continuous coal is the first goal of the survey. The RIM signal decay rate is essentially constant (once out of the near field) and any disruption to the signal can be interpreted as a RIM anomaly—in this case due to the presence of mine works affecting the ray path or geological anomalies, such as paleochannel systems. Minor variation to linear decay may occur due to slight variation in coal seam height and moisture content.

The measured signal strength of the RIM transmission was adjusted for cylindrical spreading within the seam and normalized by ray-path length to establish the attenuation rate (units of dB/100 ft). The attenuation rate was then compared for each individual ray path and for each frequency utilized during the survey. Using the location of each ray path and that path's measured attenuation rate, a contour map of in-seam signal attenuation was created for the survey area and is shown in Figure 37.

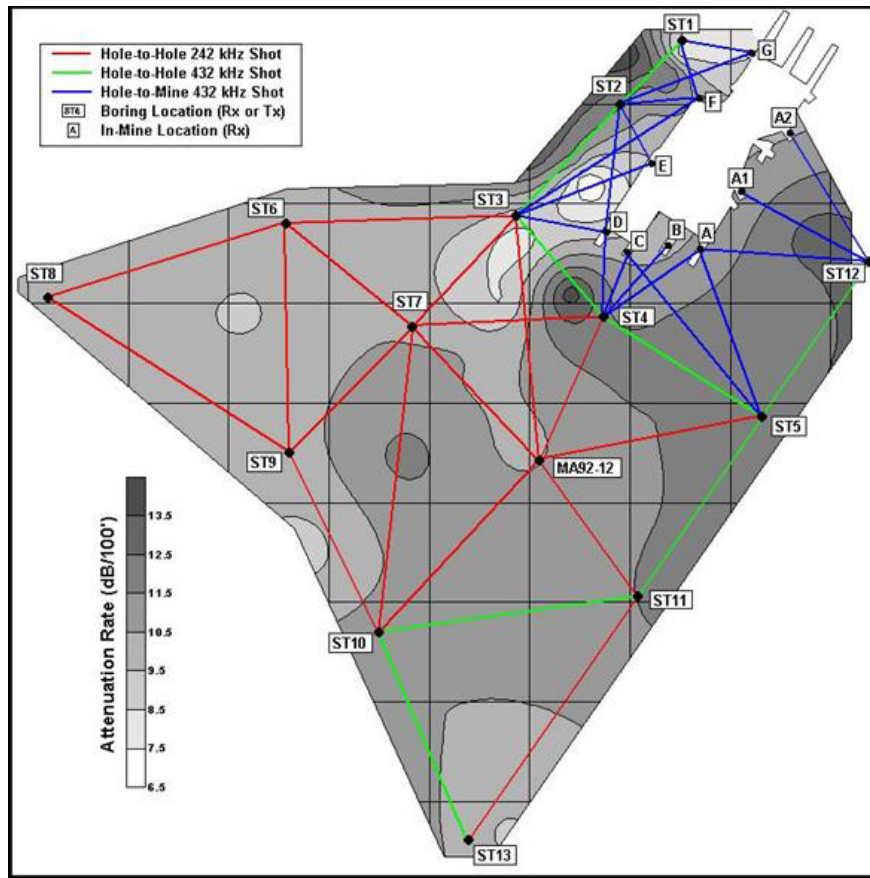


**Figure 37.** Diagram of survey area showing contour map of RIM signal attenuation rate. The contour interval is 1 dB/100 ft.

For the purpose of analysis and discussion, five distinct regions have been designated within the survey area: Region A (northwest of existing workings), Region B (southeast of existing workings), Region C (immediately in front of workings), Region D (southwest of existing workings), and Region E (further southwest of existing workings). The important conclusions are that attenuation rates measured along the perimeter of the regions indicate “solid” coal, or no voids that could be old works.

Additionally, the survey results showed high attenuation rates around and to the northwest of borehole ST4 (north is to the top of this map). As indicated in Figure 37, and confirmed by mine management, a sand channel was present in the area of high attenuation. The paleochannel scoured within the seam and introduced extremely difficult mining conditions. However, the RIM survey results indicated that the channel did not have extensive width and depth across the section. This intelligence about the anomaly was shared with management so appropriate decisions were made to continue mining operations. Once through the channel, mine management confirmed that the survey accurately predicted the physical features of the channel. Therefore, while the RIM survey’s primary purpose was to establish or confirm the barrier pillars separating the old works from active mining, management gained the added benefit of using RIM to identify and confirm adverse mining conditions.

## Void Detection and Confirmation Electromagnetic Wave Instrumentation Under Development

The Mine Safety and Health Administration (MSHA), universities with mining engineering departments, machinery manufacturers, and the mining companies have dedicated manpower to improving productivity and safety in the mining industry. The West Virginia University (WVU) International Conference on Ground Control in Mining is just one of the many technical meetings dedicated to improving safety. During the annual meeting in August 1999, the concept of incorporating real-time uncut coal thickness sensors on cutting drums was presented (28) as illustrated in Figure 38.

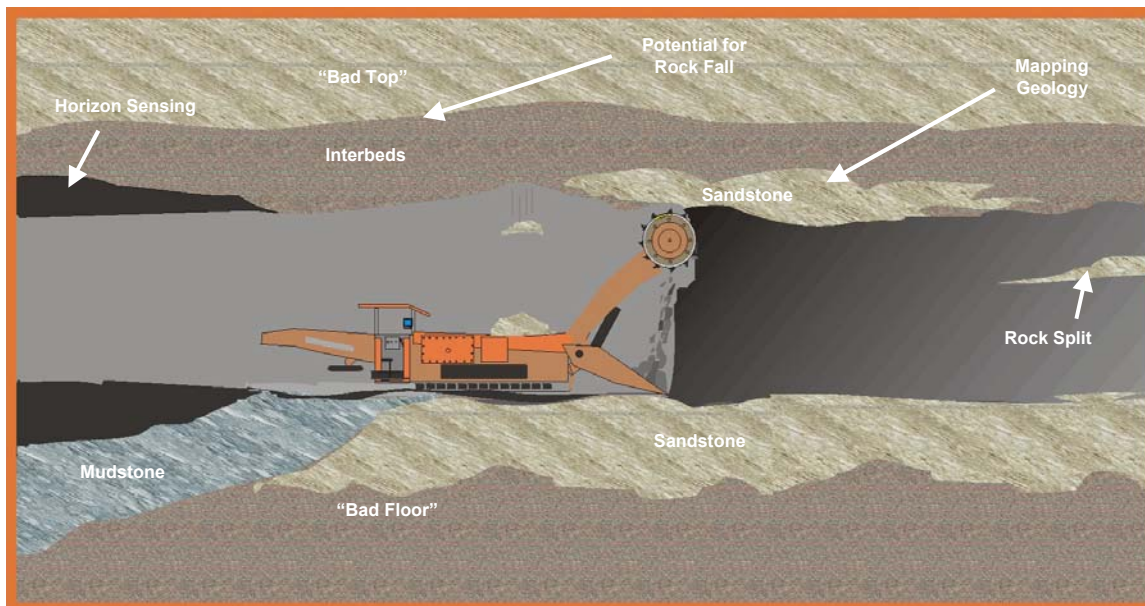


**Figure 38.** Detecting coal-rock interface horizons

The safety benefits of the drum-mounted sensor were obvious to the industry, but the technical problems appeared to be intractable. Coal cutting machines must be operated from a remote location where man interdiction is still viable. Even at these safe distances, miners are exposed to respirable dust and high acoustic noise. As illustrated above, the science of roof control can be effectively applied in unstable roof conditions by leaving roof coal. The thin layer can prevent spalling and the cutting edge from striking fragile roof rock. The drum-mounted Horizon Sensor enables real-time uncut coal thickness measurements for selective mining. The uncut coal layer will reduce the roof fall potential, especially under the margins of paleochannels. In some seams, the thin layer of roof or floor coal has higher percentages of ash, sulfur, mercury, and other heavy metals. The benefits of selective mining vary from seam to seam.

The coal-rock interface detection (CID) problem has been extensively investigated and the more promising technologies developed into experimental hardware. In the early 1970s, the

National Aeronautics and Space Administration (NASA) Marshall Space Flight Center investigation concluded that natural gamma sensors were viable for measuring uncut coal thickness (29). Bessenger and Nelson developed a gamma sensor for measuring floor coal thickness (30). Chufo (31) developed a radar with a moving antenna that proved that coal thickness and the dielectric constant could be determined from the measurement. These technical approaches were considered very successful, but could not be integrated on coal cutting drums.

During the WVU conference paper (28) question-and-answer segment, Dr. Kelvin Wu of MSHA suggested that a look-ahead capability be added to the Horizon Sensor design to enable detection of metallic gas well casing and abandoned mine entries. The concept is illustrated in Figure 39.

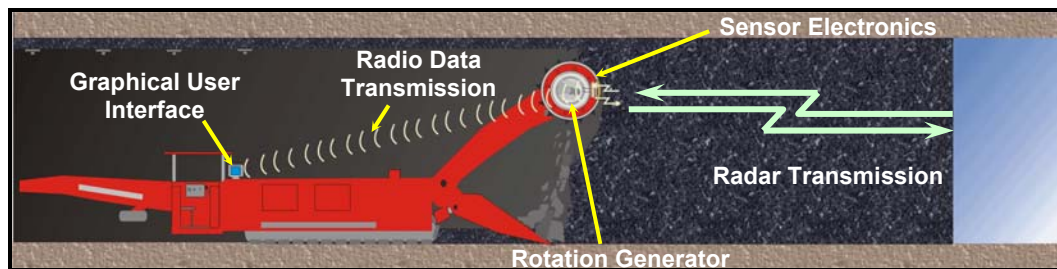


**Figure 39.** Cutting drum look-ahead radar sensor

The cutting drum-mounted sensor makes measurements when rotated 90 degrees from the look-up position.

The technical problems to be solved include the 90-g force shock and vibration levels measured on coal cutting drums.

Because continuous miner drums do not have slip rings for electric power generation, electric power must be generated on the cutting drum by electrodynamic generators (32). Measured data must be transmitted by radio data transmission between the machine body and the cutting drum. Research and development determined that a Resonant Microstrip Patch Antenna (RMPA) could be designed to withstand the coal cutting environment when enclosed in the flameproof enclosure shown in Figure 40 (33, 34).

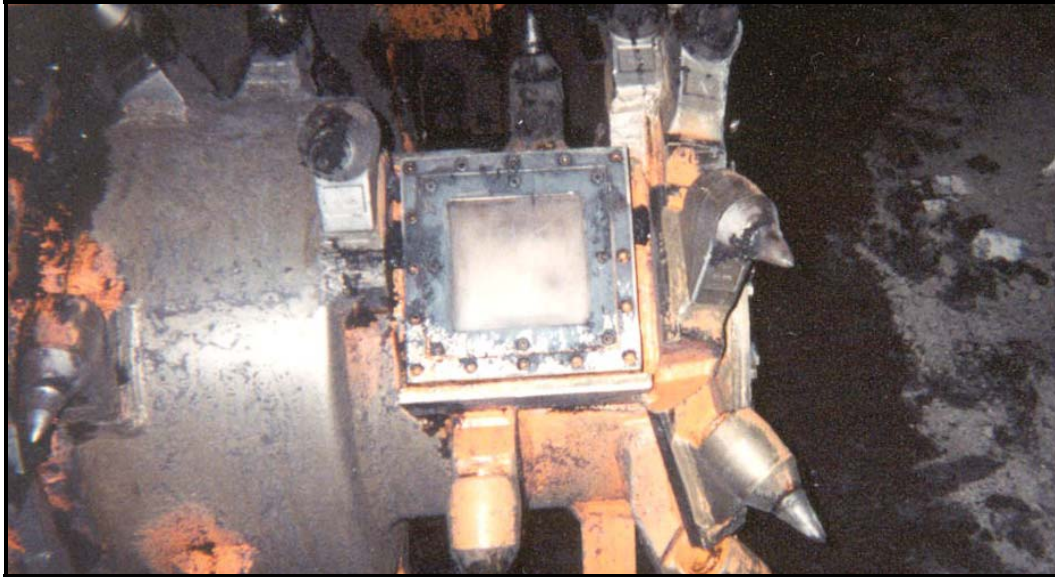


**Figure 40.** MSHA flameproof approved RMPA Horizon Sensor (HS-3) mounted on a coal cutting drum

The Horizon Sensor HS-3 has been installed on several Joy 12CM machines and operated during the past 24 months. The RMPA sensor and its resonant impedance (observable) are illustrated in Figure 41.

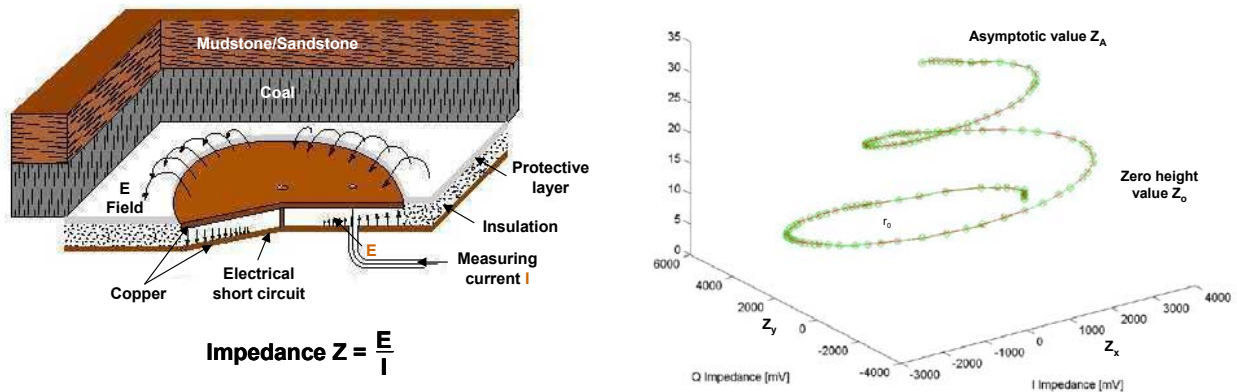


**Figure 41.** Horizon Sensor response

The Horizon Sensor RMPA generates the electric fields (magnetic fields are not shown) in the insulator between two copper plates. Along the edges of the plates, the electric fields fringe and cause a horizontally polarized electric field to travel upward through the uncut coal layer to coal-rock interface. The reflected secondary electric field returns to RMPA where the total fields and the resulting impedance are measured. The impedance is a complex number with real and imaginary parts. The HS-3 is calibrated by cutting different thicknesses of coal and measuring impedance. The sensor has a maximum thickness limitation near 40 inches. Unlike radar, the sensor measuring accuracy increases as uncut coal thickness decreases.

The Horizon Sensor instrumentation was developed and demonstrated with partial support of the Department of Energy (DOE) Mining Industry of the Future (MOF) Program. J. Michael Canty was the MOF Program Manager and Morgan H. Mosser was the acting contracting officer's representative.

The *New Yorker* magazine article (35) chronicled Dr. Kelvin Wu's competent engineering leadership role in the successful rescue of the nine trapped miners. If his 1999 vision of a cutting drum-mounted sensor with look-ahead radar capability could have become a reality by July 2002, the following photograph (Figure 42) could not have been taken.



**Figure 42.** Quecreek Mine breach (photograph courtesy of MSHA)

To evaluate the HS-3 look-ahead detection range limitation, a salt block barrier pillar simulation was set up in Stolar's laboratory. The laboratory barrier pillar simulation site was constructed with salt blocks ( $\epsilon_r = 6$ ) shown in Figure 43.

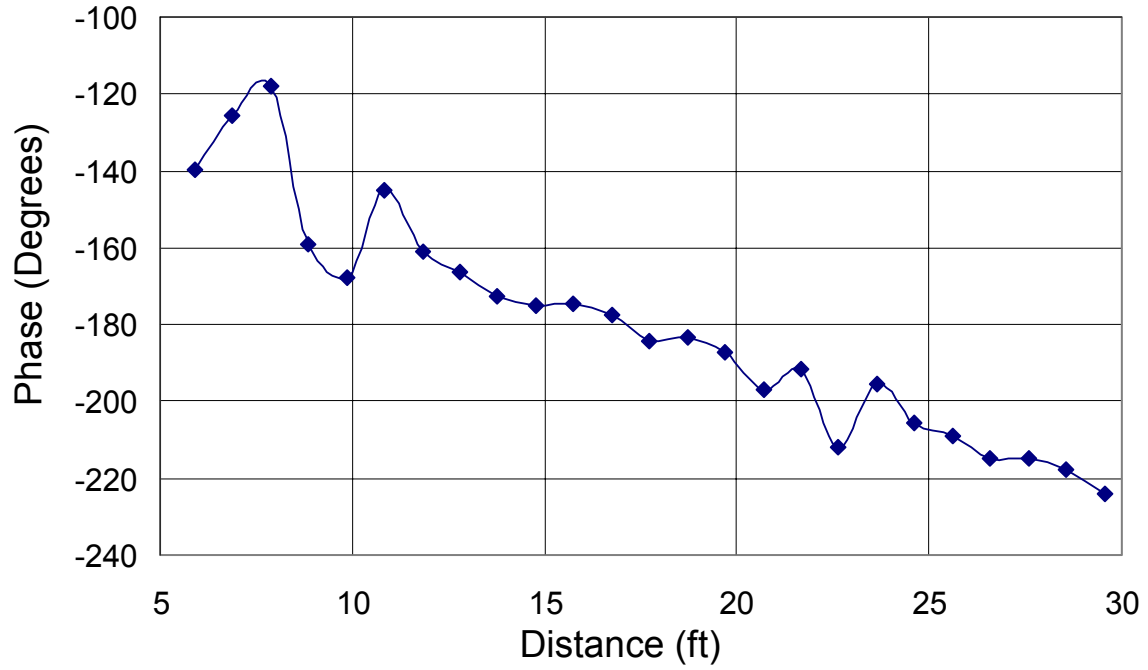


**Figure 43.** Salt block simulation of a coal barrier pillar

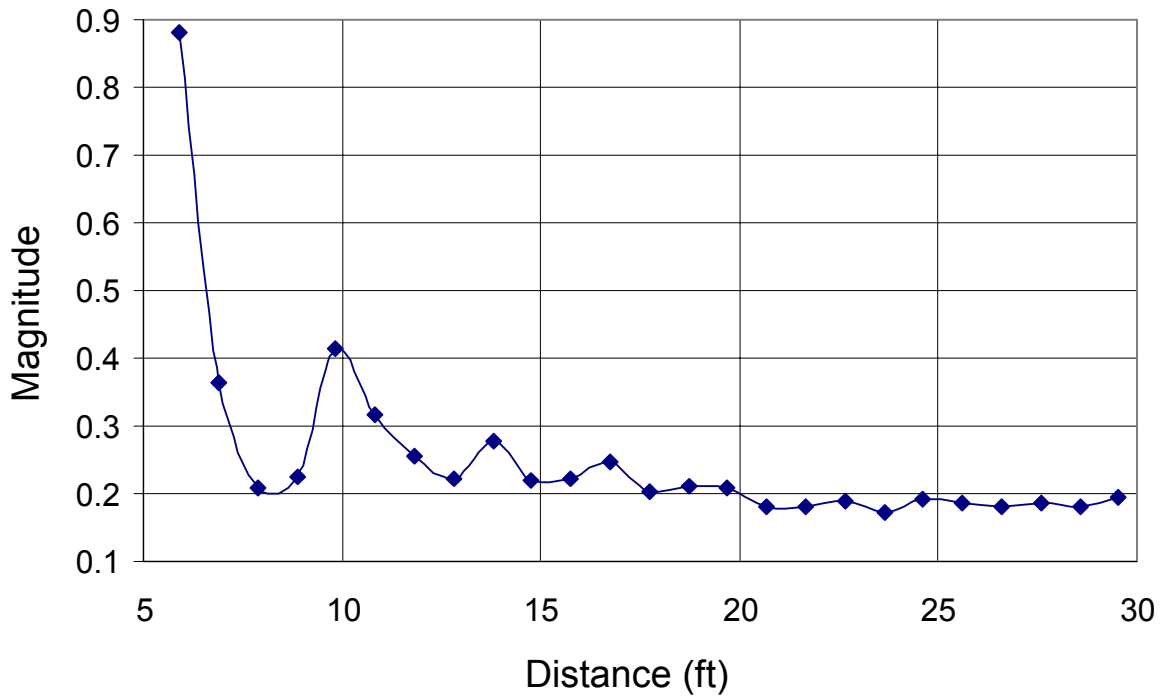
The HS-3 Horizon Sensor was rotated at the rate of 60 rpm and the HS-3 made measurements through the salt blocks to a reflector at the simulated barrier thickness. The maximum HS-3 range-detection capability was found to be 10 ft. The HS-3 computer-controlled electronics are capable of generating an automatic machine shut-down command to prevent mining into the void.

The HS-3 electronics operate in the CWSF mode to establish the resonant frequency of RMPA. Depending on the uncut thickness requirement, the RMPA frequency can be automatically set by the embedded computer to any frequency in range from 500 to more than 2500 MHz.

The HS-3 RMPA can be augmented by a wideband (non-resonant) antenna to detect far-field reflections from voids. Instruments were set up in the laboratory simulation to demonstrate range-detection capability. The CWSF radar generated 51 equally-spaced frequency steps between 0.9 and 1.1 GHz. This corresponds to a range of at least 50 ft with a 1-ft resolution. The measured radar data were processed in an FFT with the time-domain response shown in Figure 44.



(a)



(b)

**Figure 44.** Results from the experiments in salt: (a) phase and (b) magnitude response

Features close to the radar antenna are obscured due to the impulse response of the wideband radar. Most of the reflected signal's energy is concentrated at the beginning of the transformed signal, and time-gating is usually performed; this masks the response from the nearby scatterers. A change in the phase of the time-domain (impulse) response indicates the presence of a scatterer, whereas the magnitude of the impulse response corresponds to the size of the scatterer (15). The radar phase response is the observable at 23 ft. The laboratory tests confirm the feasibility of cutting drum void detection.

A necessary condition for void detection is the measurement of the coal anisotropic dielectric constant. The dielectric constant can be measured with a RMPA illustrated in Figure 45.

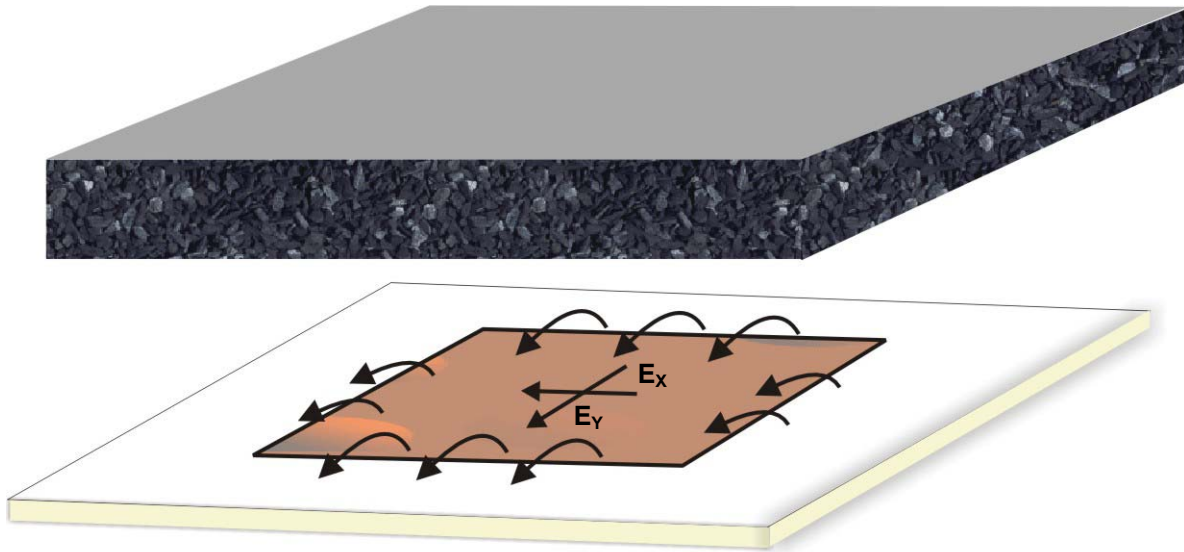


**Figure 45.** Dielectric constant measured with the Resonant Microstrip Patch Antenna (RMPA)

The RMPA driving point impedance will be measured with X-directed polarized electric fields and then Y-directed polarized electric fields. The RMPA will be integrated with cutting drum look-ahead radar antennas.

### **Proposed In-Mine Test Site**

A radar enclosed within an MSHA-approved flameproof enclosure will be used to build and demonstrate the detection of abandoned mine air-filled and water-filled entries from the working face. The demonstration will be conducted using the following in-mine demonstration site (Figure 46).

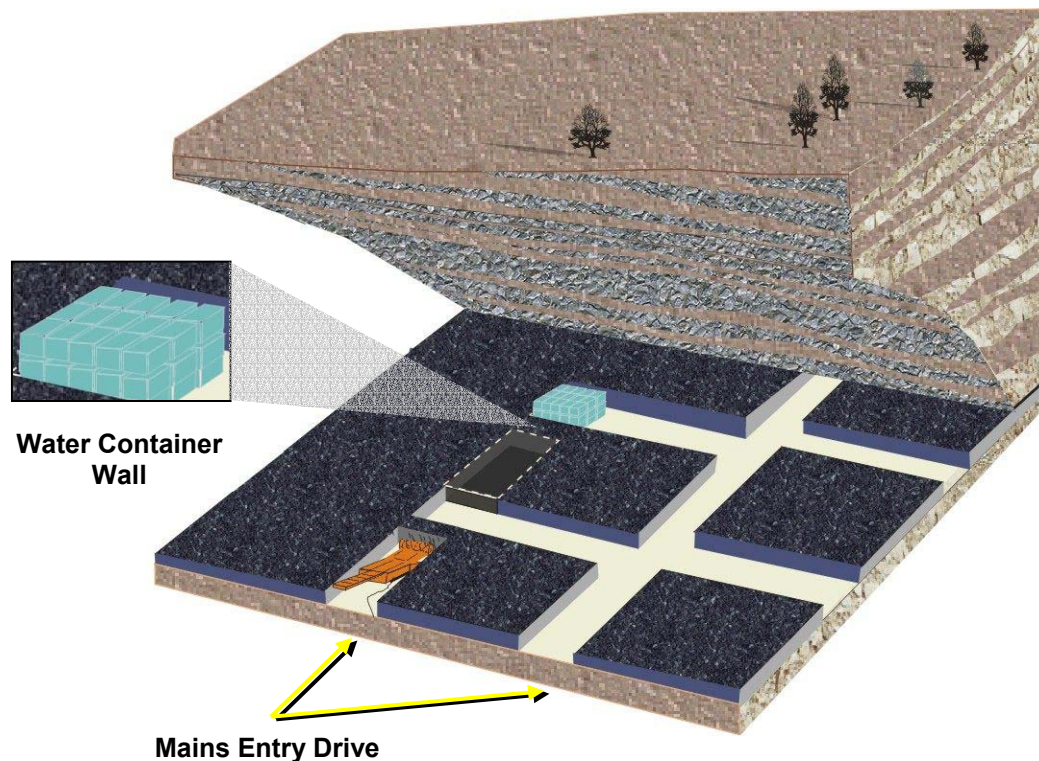


*Figure 46. In-mine demonstration site*

The continuous mining machine would first advance toward an air-filled crosscut to demonstrate detection range to a void, then advance toward a crosscut with stacked plastic water containers representing a water-filled void.

### **Drillstring Radar (DSR) for In-Seam Guidance and Navigation**

Governor Schweiker's report (27) recommended improvements in horizontal directional drilling. Real-time Measurements-While-Drilling (MWD) radar must be integrated with guidance and navigation to improve horizontal drilling. CONSOL Energy pioneered the development of horizontal drilling technology for de-gassing coal beds in advance of mining. The CONSOL instrumentation measures pitch, roll, and azimuth of the drill bit with great precision. There is no need to improve this measurement technology, which will be referred to as navigation technology. Integration of radar and relative dielectric constant instrumentation with navigation is new and will increase the horizontal drilling efficiency by more than 30%, enabling drilling along the center line in an undulating coal bed (32). The DSR can be applied through vertical drillholes to confirm the distance to the void or geologic anomaly from the borehole (Figure 47).

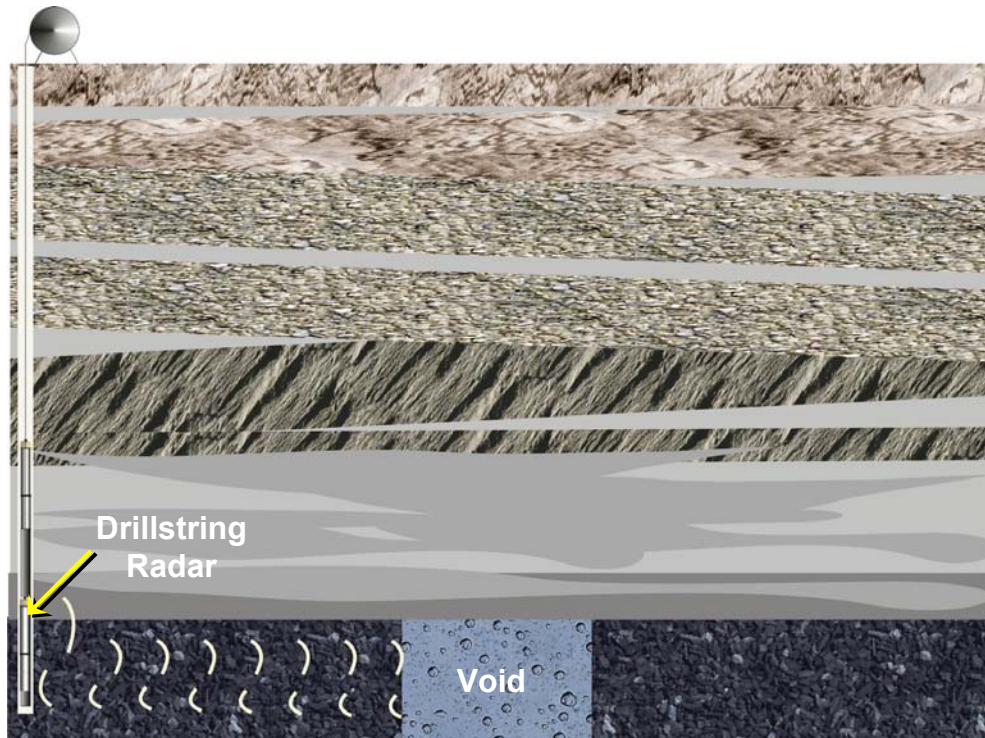


**Figure 47.** Radar mapping of voids and geologic anomalies from vertical boreholes

Abandoned mine barrier pillar verification can be achieved using directionally drilled horizontal boreholes as illustrated in Figure 48.

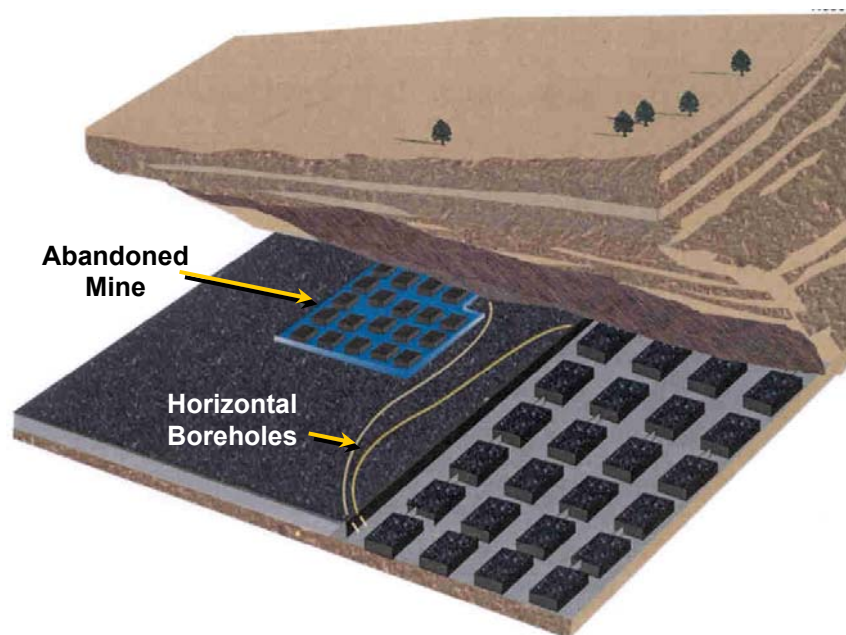


**Figure 48.** Detection and imaging of abandoned coal mines along boreholes

Horizontal boreholes can establish that a safe barrier pillar of coal exists between the borehole and the mine development. The boreholes would be drilled parallel to and 30 ft away from a suspected abandoned mine boundary. Mining would be allowed to approach no closer than 50 ft to the directionally drilled horizontal hole. Radar and navigation instrumentation integrated into the drillstring would be used to measure the distance to the abandoned mine voids and the mine development entries.

Surface directional drilling technology for de-gasification of coal beds in advance of mining has been achieved in Australia and Appalachian coal basins. Vertical borehole segments are drilled to a predetermined depth and then directional drilling a 90-degree curve to intercept the coal bed horizontally.

### **Current In-Seam Drilling Technology**

Current MWD navigation systems are used to guide in-seam drilling in coal deposits, but these systems cannot directly determine seam thickness or distance to a void or changes in seam orientation (e.g., dips and rolls) without employing a time-consuming sequence of drilling to the floor and then to the roof or vice versa in the same region of the panel, commonly called sidetracks (see Figure 49). The drilling machine operator is only able to detect when the drill is on the roof or floor horizon by the evidence of rock in the cuttings. Once these situations are detected, the operator redirects the drill motor in an appropriate drillstring rotation angle to realign the drill within the seam. A down-the-hole drill motor used in horizontal drilling applications is also shown in Figure 49.

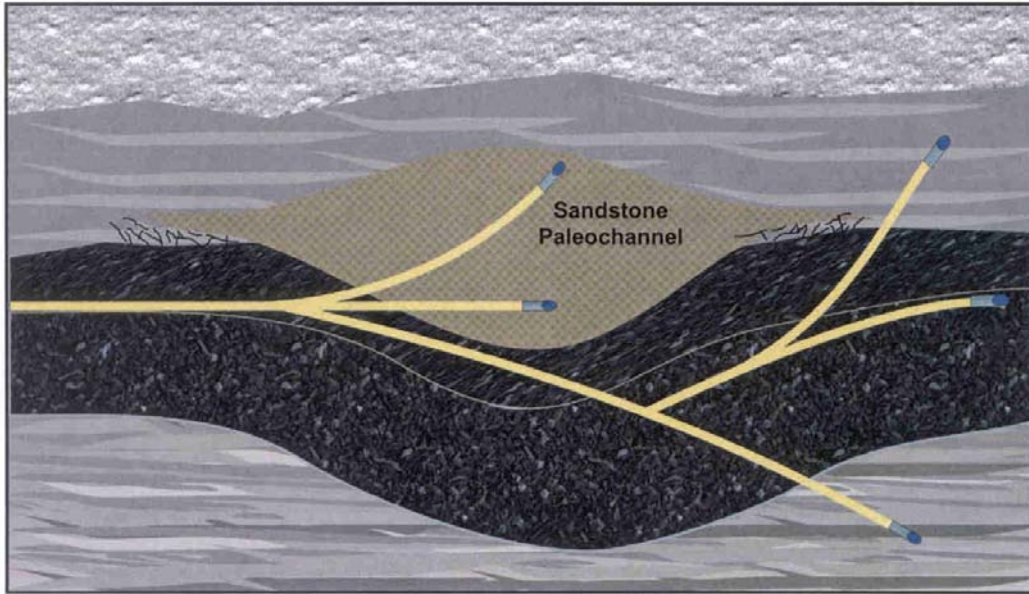


**Figure 49.** Vertical cross section of a coal bed illustrating conventional “sidetrack” trial-and-error drilling under a paleochannel as well as the down-the-hole drill motor

The current directional drilling with a bent sub has a minimum seam height limitation. A controlled gimbal would enable drilling in thinner coal beds.

## Basic Structure of the Drillstring Radar (DSR) Tool

The drillstring radar (DSR) has been designed to be installed inside a conventional drillrod as shown in Figure 50.

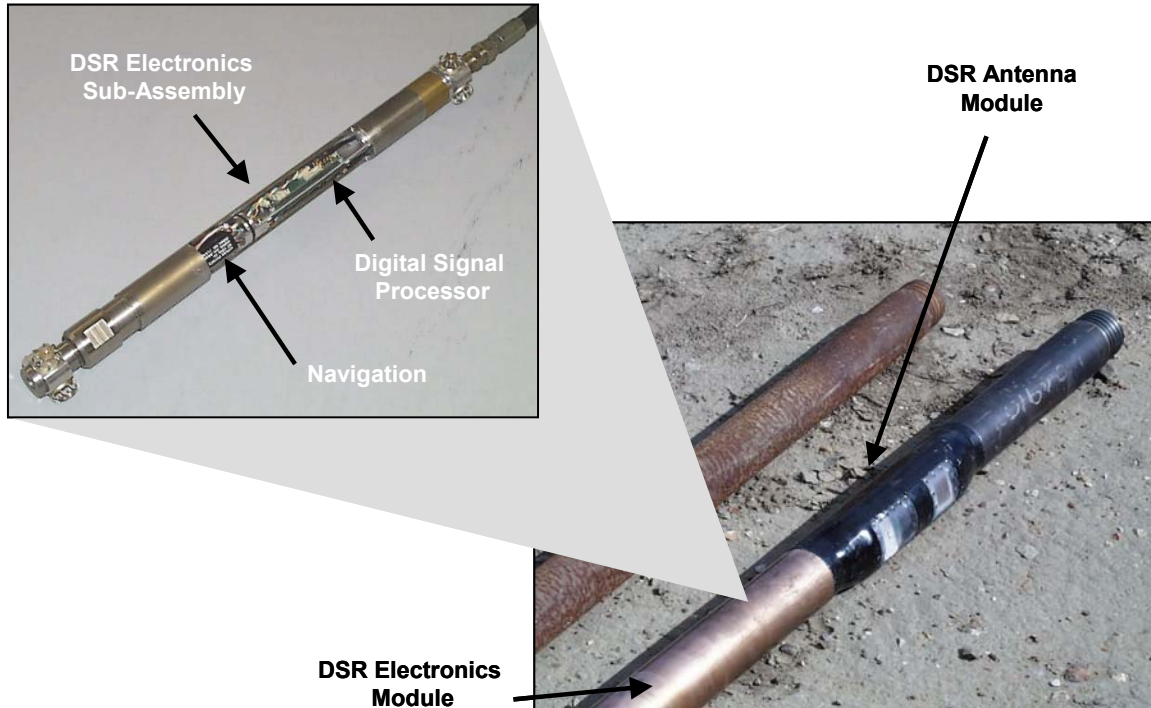


**Figure 50.** Stolar Drillstring Radar (DSR)

The radar electronics are installed in a retractable titanium flameproof enclosure (36, 37). The enclosure has passed the MSHA flameproof investigation. A battery pack (under MSHA I/S investigation) will be replaced by a hydroturbine. An inductive radio provided data transmission along the drillstring.

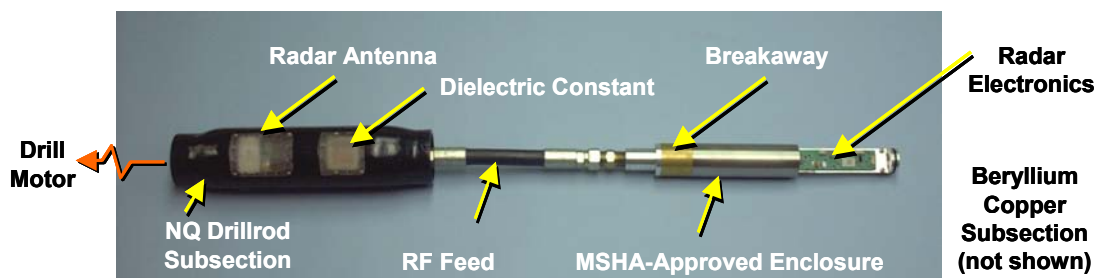


**Figure 51.** Measurements-While-Drilling (MWD) drillstring radar

A block diagram of the DSR instrument system is given in Figure 52.

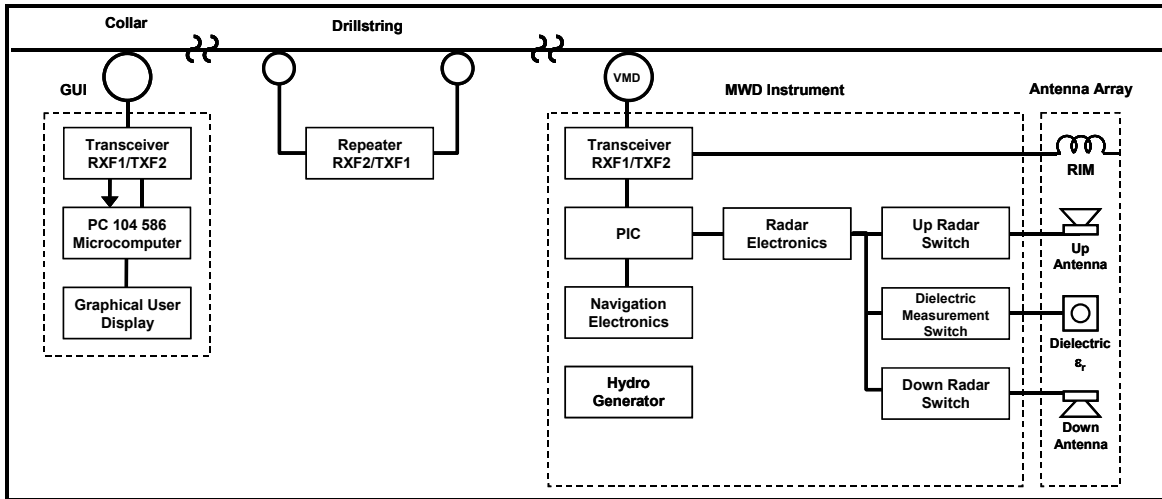


**Figure 52.** Block diagram of the drillstring radar instrumentation system

The MWD subsection of the DSR technology includes: (1) radar electronics for determining the distances from the horizontal boring to the roof/floor sedimentary rock layer and void, (2) navigation electronics for mapping the direction of the boring, and (3) drillstring data transmission hardware for transmitting processed radar and navigation information to the drilling machine.

The MWD instrumentation includes a coal seam waveguide imaging signal transmitter. A companion receiver in a prior-drilled horizontal borehole acquires RIM-IV data for tomographic processing.

The DSR technology features a downhole MWD instrument docked inside a beryllium copper drillrod subsection. This drillrod subsection is next to the antenna array drillrod subsection. For surface-based drilling, an F1/F2 repeater is deployed in the middle of the vertical section of the drillstring. At the collar, a GUI will log and process measured data. The graphical display will show the vertical cross section of the coal seam, the seam height, and type of boundary rock along the drillhole. The display will also include a plan view showing the heading of the drillhole.

## **Major Subsystems**

- (1) GUI with data logging and processing software
- (2) Two-way radio data transmission subsystem for communications along the drillstring
- (3) MWD instrument to acquire data and transmit the data to the collar
  - Radar to map seam height and type of boundary rock along the path of the drill
  - Navigation instrument to measure heading of the horizontal drill pitch, yaw, and rotation angle of the drilling subsection
- (4) RIM-IV instrumentation for crosshole measurement

## Concluding Remarks

This paper has been written for decision makers concerned with enhancing safety and productivity in the coal mining industry. The mining industry has achieved impressive safety and productivity improvements in recent years. Productivity has improved between 6 and 7% per year (38–40) for many years; safety has exceeded the pace.

The deterioration in US coal reserves and the spoiling of coal beds with the aggressive cavitation method of coal bed methane (CBM) production calls into question the continuation of productivity improvement. In future years, electromagnetic (EM) wave technologies will play a vital role in continuing the safety and productivity improvement through coal seam vision. From a safety point of view, abandoned mines and gas well casings are mining hazards that impact safety in recognizable ways. Anomalous geology presents even greater safety issues. Oftentimes, paleochannels scouring into the sedimentary roof rock weaken the seam boundary rock. Channels have caused ground control problems that have indirectly caused significant loss. For these reasons, we have expanded the scope of this paper beyond the detection of voids to include geologic anomalies.

EM wave vision requires the cognitive processes of detection, confirmation, and mitigation. EM wave technologies solve the detection problem. Imaging forms a silhouette of the void or geologic anomaly, while advanced horizontal drilling is essential to the confirmation process. Imaging is a targeting technology for advanced drilling. Hazard mitigation improves because the science of ground control can be appropriately applied in anomalous geologic zones. This science, along with horizon control under the margins of paleochannels, will improve safety and productivity, and prevent future accidents such as the Quecreek mine inundation. Also, with improved barrier confirmation, pillars can be reduced eliminating some coal sterilization.

The case study proves the points being made in these remarks. The goal of the RIM barrier pillar survey was to determine the pillar integrity. An additional benefit was realized by the detection of a paleochannel ahead of mining and the better knowledge that clear coal followed the channel scours. The image and improved intelligence about the geology prevented the mine from shutting down, increasing coal recovery from the reserve.

## References

1. King, R. W. P., and S. Prasad. 1986. *Fundamental Electromagnetic Theory and Applications*. Englewood Cliffs, New Jersey: Prentice-Hall, Inc.
2. Wait, J. R. (ed.). 1971. *Electromagnetic Probing in Geophysics*. Boulder, Colorado: The Golem Press.
3. Wait, J. R. 1982. *Geo-Electromagnetism*. New York, New York: Academic Press, a Subsidiary of Harcourt Brace Jovanovich, Publishers.
4. Wait, J. R., and D. A. Hill. 1976. "Analytical Investigation of Electromagnetic fields in Mine Environments" (Contract H0155088, NOAA, US Dept. Commerce), BuMines OFR 53-77, Nov. 15, 200 pp.
5. Stratton, J. A. 1941. *Electromagnetic Theory*. New York and London: McGraw-Hill Book Company, Inc.
6. Vozoff, K. G. (ed.). 1985. *Magnetotelluric Methods Geophysics*. Reprint Series No. 5. Society of Exploration Geophysicists.
7. Van Bladel, J. 1964. *Electromagnetic Fields*. New York, San Francisco, Toronto, London: McGraw-Hill Book Company.
8. Collin, R. E., and F. J. Zucker. 1969. *Antenna Theory, Part 2*. New York, St. Louis, San Francisco, London, Sydney, Toronto, Mexico, Panama: McGraw-Hill Book Company.
9. Wait, J. R. 1963. "The Possibility of Guided Electromagnetic Waves in the Earth's Crust." *IEEE Transactions on Antennas and Propagation*.
10. Stolarczyk, L. G. 2001. Detection and Characterization of Underground Facilities with Synchronized EM Gradiometer Transponders. US Patent 6,549,012B2, filed July 12, 2001, and issued April 15, 2003.
11. Kelly, R. E. 1999. "Electromagnetic Detection of Underground Structures." LDRD final report LA-UR-99 2117. Presented at American Geophysical Union, San Francisco, California, December 2000, and at Society of Optical Engineers (SPIE) in San Diego, California, July 2001.
12. Nahin, P. J. 1987, 1988. *Oliver Heaviside, Sage in Solitude: the Life, Work, and Times of an Electrical Genius of the Victorian Age*. New York: IEEE Press.
13. Berube, D., F. M. Ghannouchi, and P. Savard. October 1996. "A Comparative Study of Four Open-Ended Coaxial Probe Models for Permittivity Measurements of Lossy Dielectric/Biological Materials at Microwave Frequencies." *IEEE Transactions on Microwave Theory and Techniques*, Vol. 44, No. 10.

## References (continued)

14. Balanis, C. A. 1982. *Antenna Theory Analysis and Design*. New York: John Wiley & Sons.
15. Skolnik, M. I., *Introduction to Radar Systems*, New York, McGraw-Hill, 1962
16. Middleton, D. 1987. *An Introduction to Statistical Communication Theory*. Los Altos, California: Peninsula Publishing.
17. Cook, J. C. 1974. "Radar Transparencies of Mine and Tunnel Rocks." Paper presented at the 44<sup>th</sup> Annual International SEG Meeting, November 12, 1974, Dallas, Texas. *Geophysics*, Vol. 40, No. 5 (October 1975). p. 865–885.
18. Gardner, D., J. Guerrier, and M. Martinez. 1994. "Ground Penetrating Radar Coal Measurements Demonstration at the U.S. Bureau of Mines Research Center, Pittsburgh, Pennsylvania." Final Report. EGG 11265-3015 UC-906.
19. Hill, D. 1984. "Radio Propagation in a Coal Seam and the Inverse Problem." *Journal of Research*, National Bureau of Standards, Vol. 89, No. 5, Sept.–Oct.
20. Stolarczyk, L. G., and R. C. Fry. 1990. "Radio Imaging Method (RIM) or diagnostic imaging of anomalous geologic structures in coal seam waveguides." *Transactions of Society for Mining, Metallurgy, and Exploration, Inc.*, Vol. 288, 1806–1814.
21. Stolarczyk, L. G. 1986. Continuous Wave Medium Frequency Signal Transmission Survey Procedure for Imaging Structure in Coal Seams. US Patent RE 32,563, filed July 28, 1986, and issued December 15, 1987.
22. Stolarczyk, L. G. 1985. Electromagnetic Instruments for Imaging Structure in Geologic Formations. US Patent 4,691,166, filed December 23, 1985, and issued September 1, 1987.
23. Stolarczyk, L. G. 1985. "Continuous Wave Medium Frequency Signal Transmission Survey Procedures for Imaging Structures in Coal Seams." US Patent 4,577,153, filed May 6, 1985, and issued March 18, 1986.
24. Thomson, S., P. Hatherly, and G. Liu. 1990. "The RIM I in-mine method – Theoretical and applied studies of its mine exploration capabilities." *The Coal Journal*, Vol. 29, p. 33–40.
25. Vozoff, K., G. Smith, P. Hatherly, and S. Thomson. 1993. "An Overview of the Radio Imaging Method in Australian coal mining." *First Break*, Vol. 10(1).
26. Stolarczyk, L. G., S. Peng, and Y. Luo. 2003. "Imaging Ahead of Mining with RIM-IV Instrumentation and 3-D Tomography Software." In proceedings of the 22<sup>nd</sup> International Conference on Ground Control in Mining, p. 136–143.
27. Report of Commission on Abandoned Mine Voids and Mine Safety. November 15, 2002. <http://www.dep.state.pa.us/hosting/minesafetycommission/default.htm> (accessed July 22, 2003)

## References (concluded)

28. Stolarczyk, L. G. 1999. "Electromagnetic Seam Wave Mapping of Roof Rock Conditions Across a Longwall Panel." In Proceedings of the 18<sup>th</sup> International Conference on Ground Control in Mining, p. 50–53.
29. Stolarczyk, L. G., G. L. Stolarczyk, and K. L. Perry. 1996. "Horizon Sensor for Advanced Coal Extraction (ACE)." Presented at National Mining Association MINExpo International '96, Las Vegas, Nevada.
30. Bessenger, S. L., and M. E. Nelson. 1990. "Remnant Roof Coal Thickness Measurements with Passive Gamma Ray Instrumentation in Coal Mining." Proceedings of the IEEE/IAS Annual Meeting, Seattle, Washington.
31. Chufo, R. L., and W. I. Johnson. 1991. "A Radar Coal Thickness Sensor." Proceedings of the 1991 IEEE Industry Applications Society Annual Meeting, Dearborn, Michigan.
32. Stolarczyk, L. G., G. L. Stolarczyk, and D. L. Baldrige. 1991. Method for Controlling the Thickness of a Layer of Material in a Seam. US Patent 5,188,426, filed September 11, 1991, and issued February 23, 1993.
33. Stolarczyk, L. G., G. L. Stolarczyk, and D. L. Baldrige. 1989. Method and Apparatus for Measuring the Thickness of a Layer of Geologic Material using a Microstrip Antenna. US Patent 5,072,172, filed August 30, 1989, and issued December 10, 1991.
34. Stolarczyk, L. G. 1996. Method and Apparatus for a Rotating Cutting Drum or Arm Mounted with Paired Opposite Circular Polarized Antennas and Resonant Microstrip Patch Transceiver for Measuring Coal, Trona, and Potash Layers Forward, Side, and Around a Continuous Mining Machine. US Patent 5,769,503, filed July 23, 1996, and issued June 23, 1998.
35. Boyer, P. J. "Rescue at Quecreek." *The New Yorker*, November 18, 2002, p. 56–73.
36. Stolarczyk, L. G. 2001. Drillstring Radar. US Patent application, filed August 28, 2001.
37. Stolarczyk, L. G. 2001. Ground-Penetrating Imaging and Detection Radar. US Patent 6,522,285B2, filed March 28, 2001, and issued February 18, 2003.
38. Stolarczyk, L. G., G. G. Wattlely, and A. P. Schissler. "The World of Smart Mining." *World Coal*, May 2001.
39. Stolarczyk, L. G., and G. G. Wattlely. "Breakthrough Technology." *World Coal*, May 2002.
40. Stolarczyk, L. G., and G. G. Wattlely. "Sensing the Future." *World Coal*, May 2003.

## Acknowledgments

The advanced development of the Horizon Sensor and Radio Imaging Method (RIM) instrumentation was partially sponsored by the Department of Energy (DOE) Mining Industry of the Future (MOF) and Initiative for Proliferation Prevention (IPP) programs. Dr. Hooman M. Tehrani contributed to the development of the antennas. The authors want to thank Gerald L. Stolarczyk and Igor Bausov for their work on development of the instrumentation. Senior Geophysicist Joseph T. Duncan conducted the in-mine demonstration programs. He was supported in this effort by Bruce Ley, Randy L. Acre, and John A. Myers.

The DOE IPP drillstring radar (DSR) program is administered by Dr. Chris Baumgart, Chris Miller, and Ashot Tumagyan of the DOE's Kansas City Plant Albuquerque Office. Approximately 150 scientists and engineers are working at the MINATOM Sedakov Institute for Measuring Systems Research on development of software and associated radar electronics.

Special appreciation is given to Jerry Jones and Daniel Carreon for the development of the manufacturing and quality-control processes used in building the instrumentation. Special recognition is extended to Dan Gregory and the structural dynamic engineering staff at Sandia National Laboratories for helping solve the 100-g shock and vibration sustainability of the drum-mounted Horizon Sensor. Glenn Rightmire, retired Professor of Mechanical Engineering at Columbia University, contributed to the solution of the shock and vibration problem.

The authors want to extend their special thanks to Glenn G. Wattley for managing the product launch and maintaining mining industry relationships during the field test program. Randy L. Acre provided valuable assistance in developing the sales and field support strategies for the in-mine installations.

The underground demonstration of the Horizon Sensor and RIM technologies was in part sponsored by the DOE MOF program. J. Michael Canty was the Program Manager and Morgan H. Mosser was the acting contracting officer's representative. The Horizon Sensor received the 2002 R&D 100 Award. The Chief Executive Officers of the NMA developed the hierarchy of technology needs for the DOE MOF program. The technical staff of the following NMA mining companies participated in the in-mine demonstrations: InterWest Mining, RAG American Coal Company, CONSOL Energy, and West Elk, a unit of Arch Coal, Inc. The following non-NMA companies also participated: Oxbow Coal Mining, The Ohio Valley Coal Company, Exxon Monterey Coal, and Blue Mountain Energy.

The authors want to thank Jeannie Pomeroy for preparing the manuscript, and Steve Bertola for the illustrations.